AIMS Materials Science, 11(5): 882–917.
DOI: 10.3934/matersci.2024043
Received: 09 August 2024
Revised: 22 September 2024
Accepted: 29 September 2024
Published: 09 October 2024

http://www.aimspress.com/journal/Materials

Research article

Influence of graphene nanoplatelets (GNPs) and aluminum-carbon layered double hydroxides (Al-C LDH) in polypropylene matrix of hybrid composite structures on the microstructure and mechanical performances

R. Daulath Banu[1], R. Karunanithi[2,*], S. Sivasankaran[3], B. Subramanian[4] and Abdullah A. Alhomidan[5]

[1] Department of Polymer Engineering, B. S. Abdur Rahman Crescent Institute of Science and Technology, Chennai 600048, India
[2] Department of Mechanical Engineering, B. S. Abdur Rahman Crescent Institute of Science and Technology, Chennai 600048, India
[3] Department of Mechanical Engineering, College of Engineering, Qassim University, Buraydah 51452, Saudi Arabia
[4] Electroplating and Metal Finishing division, CSIR, Central Electro Chemical Research Institute, Karaikudi 600003, Tamilnadu, India
[5] Department of Mechanical Engineering, College of Engineering, University of Akron, Ohio 44325-3903, United States

* **Correspondence:** Email: karunaponni@gmail.com; karunanithi@crescent.education.

Abstract: In this study, a polypropylene (PP) matrix was reinforced with ultra-fine graphene nanoplatelets (GNPs), aluminum-carbon layered double hydroxides (Al-C LDHs), and calcium carbonate ($CaCO_3$) as hybrid reinforcements, along with polypropylene grafted maleic anhydride (PP-g-MA) compatibilizers to create a novel thermoplastic-based hybrid composite polymer. The hybrid composite consisted of varying weight percentages of GNPs (ranging from 0.5 to 2.0 wt% in increments of 0.5), 2wt% Al-C LDH, 2wt % $CaCO_3$, and 5wt % PP-g-MA. The bulk samples were manufactured using twin-screw extrusion followed by vertical injection molding. The developed hybrid composites were characterized using high-resolution scanning electron microscopy (HRSEM) for microstructural analysis, X-ray diffraction (XRD) for phase identification, X-ray photoelectron

spectroscopy (XPS) for compositional analysis, and Fourier-transform infrared spectroscopy (FTIR) for functional group identification. Thermogravimetric analysis (TGA) was performed to assess thermal stability, crystallization, and melting behavior. Mechanical tests, including tensile, compressive, and three-point bending, were conducted to evaluate mechanical properties, while a low-velocity impact test assessed impact resistance. The results showed that the hybrid composite with a PP matrix embedded with 1.5 wt% GNPs, 2 wt% Al-C LDH, and 2 wt% $CaCO_3$ exhibited improved mechanical properties, achieving an ultimate tensile strength of approximately 45 MPa. This enhancement is attributed to the effective interconnection, bonding, and cross-linking of the reinforcements with the PP matrix, facilitating efficient load transfer, which makes it suitable for structural applications.

Keywords: thermoplastic matrix; GNPs/Al-C LDH; hybrid composite; polypropylene; mechanical and thermal properties

Abbreviations: PP: Polypropylene; PP-g-MA: Polypropylene grafted maleic anhydride; GNPs: Graphene nanoplatelets; Al-C LDH: Aluminum-carbon layered double hydroxides; $CaCO_3$: Calcium carbonate; FEG-HRSEM: Field emission gun high-resolution scanning electron microscopy; XRD: X-ray diffraction; XPS: X-ray photoelectron spectroscopy; FTIR: Fourier-transform infrared spectroscopy; TGA: Thermogravimetric analysis

1. Introduction

Polymeric materials are widely used across various industrial sectors due to their exceptional qualities and low cost [1]. However, their relatively weak mechanical properties make them susceptible to surface scratches, raising concerns about quality. These scratches can significantly impact the integrity, durability, and aesthetics of consumer goods, potentially limiting their industrial applications. The process of scratching or marring in polymeric materials is a common issue, influenced by the geometry of the indenter and the interaction between the material and the indenter on the surface. As a result, considerable attention has been given to scratch testing of polymers over the past few decades. Various types of scratch-induced damage have been reported, including material loss, surface chipping, periodic cracking, and marring, depending on the material's characteristics and the applied stress conditions [1,2].

Polymeric materials exhibit different mechanical properties, such as modulus, stiffness, and flexural strength, which depend on their molecular weight and the microstructures of incorporated elements [3]. These materials can be either brittle or ductile. Fillers and reinforcement materials like talc [4–8], glass beads [7], glass fiber, rubber [8], flax [9], and minerals in the form of micro-particles [10–12] are commonly added to enhance mechanical properties. Consequently, the characteristics of polymeric materials become more complex, leading to variations in their scratch and surface responses, making their scratch behavior unpredictable. Additionally, the scratch resistance of polymer materials is significantly influenced by the shape of the indenter [13]. Sharp indenters tend to cause more brittle failure and deeper scratches. A wide variety of indenter types and sizes are used in real-world applications, which can present challenges. Polypropylene (PP) is one of the most widely used commodity polymers, known for being cost-effective and offering a favorable combination of

properties, including good mechanical strength, easy processability, and recyclability. However, drawbacks such as poor low-temperature impact strength, surface crazing after repetitive flexing, and weak scratch resistance can limit its applications [14,15]. Moreover, it is well known that processing conditions significantly affect the mechanical properties of PP [15–17].

There is significant interest in using PP as a substitute for acrylonitrile butadiene styrene (ABS) in the automotive sector to facilitate recycling. However, research has shown that PP is prone to surface damage, such as marring and scratching, which limits its potential as a replacement. Reducing scratch visibility and increasing scratch resistance is crucial from an aesthetic standpoint. The appearance of scratches depends on their size, depth, and width, as well as factors like stress whitening and the underlying deformation mechanisms. Scratches can weaken polymeric materials by reducing their mechanical strength and serving as stress concentration points. Inherent properties, such as toughness, modulus, yield stress, isotacticity, and molecular chain length, play a key role in determining scratch resistance [18,19]. Extrinsic factors, including the coefficient of friction, indenter geometry, temperature, and strain rate, also significantly impact scratch performance. Additionally, the use of lubricants, stiff filler particles, and elastomers can further influence scratch resistance.

Dasari et al. [20] found that short-chain polymers resist scratch deformation better than long-chain polymers. They also showed that increased crystallinity enhances scratch resistance in polymers. According to Xiang et al. [6], a higher coefficient of friction increases the likelihood of crazing, debonding, cracking, and cavitation, suggesting that reducing friction can help minimize scratch damage. Improvements in yield stress and modulus positively affect the scratch resistance of PP. Researchers have investigated the effects of micro-fillers such as mica, wollastonite, and talc on the scratch resistance of PP [21]. Various methods have been developed to assess polymer scratch resistance, usually involving an indenter that scratches the polymer under a specific load and speed, followed by measuring one of the scratch dimensions. Some researchers use a scratch hardness criterion, evaluating scratch resistance based on scratch width and the applied force [6,18].

Scratch and stain resistance in both exterior and interior components is a critical factor that influences customers' perceptions of product value and quality. PP is an ideal material for these parts due to its distinct advantages. In automotive engineering, composite materials are increasingly favored for weight reduction because of their versatile applications. The development of materials with novel characteristics is particularly appealing, and hybridization offers an effective solution to certain challenges. The simple manufacturing process of hybrid composites allows for the enhancement of functional properties by replacing conventional materials. However, achieving a balance of composite characteristics is essential [22,23].

Graphene nanoplatelets (GNPs) have become an affordable and readily available filler for polymer-matrix nanocomposites. GNPs are easier and cheaper to synthesize compared to single-layer graphene or carbon nanotubes, making them a preferred choice [24]. GNPs possess a range of attractive properties, including a high aspect ratio, low weight, mechanical toughness, cost-effectiveness, and excellent thermal and electrical conductivity, all within a planar structure. These characteristics make GNPs a compelling alternative to many other nano-fillers in materials science, such as metallic nanoparticles, clay, and other carbon allotropes like carbon nanotubes or carbon black [25]. GNPs can be effectively and easily incorporated into polymer matrices through solvent or melt compounding, which makes them desirable for use in nanocomposites [26]. Polymer/graphene nanocomposites exhibit superior mechanical, electrical, thermal, gas barrier, and flame-retardant properties compared to conventional polymers. Additionally, graphene-based polymer nanocomposites demonstrate

significantly better mechanical and electrical performance than those based on clay or other carbon fillers. Even small concentrations of GNPs can significantly alter the properties of the polymer matrix [27,28]. Several recent studies have focused on the mechanical properties of polymer/GNP composites, though a key challenge remains in achieving uniform GNP dispersion within the composite, as this directly affects performance. The preparation method plays a crucial role in determining the quality of GNP dispersion.

Layered double hydroxides (LDHs) possess tunable characteristics that make them promising materials for a wide range of applications. Allmann and Taylor were the first to address the structure and properties of LDHs [29]. LDHs have been used for many years as multifunctional materials due to their simple synthesis methods, the availability of various sources and technologies, and their potential for structural modifications, such as alterations in layers or cation combinations. The structure of LDHs can be modified in several ways, including changes to the metallic cations, compositions, metal combinations, or interlayer anions. The metals comprising the structure and the synthesis process are key factors that determine the application and use of LDHs [30]. LDHs with various metallic compositions can be synthesized using processes such as ion exchange, hydrothermal synthesis, urea hydrolysis, and co-precipitation. They have been used in numerous applications, including in the pharmaceutical [31] and biomedical [32] fields, wastewater treatment [33], as acid scavengers [34], antioxidants [35], catalysts [36], UV-Vis absorption materials, flame retardants [37], and polymer stabilizers [38]. LDHs are also employed in solar and photovoltaic cells [39], supercapacitors [40], and sensors [41]. Additionally, LDHs find applications in other sectors, such as coolants and diluents for flammable gases [42] and as flame-retardant supports in polymers, helping to resist ignition, provide alternative combustion pathways with slower flame spread rates, and reduce smoke production [43]. Jiang et al. [44] used organically modified ZnAl LDHs with Zr 2-(2-(2-aminoethylamino) ethylamino) ethylphosphonate (ZrP) to enhance the flame retardancy of PP. Qiu et al. [45] investigated the thermal and flame-resistant characteristics of PP nanocomposites containing organically modified MgAl LDHs. The PP/stearic LDH (24 h) composite, with a 20 wt% loading of LDHs, demonstrated the best flame-retardant performance.

Ghabezi et al. [46] fabricated thermoset composites using epoxy and nanofillers (alpha and gamma grades of nano alumina). The nanofillers were heated in an oven in two stages: first, for 150 min at 80 °C, followed by 150 min at 120 °C. Epoxy composite samples were prepared with varying weight percentages of nanofillers (1%–6%). The resin nanoparticles were mechanically mixed and then heated at 50 °C in an oven, followed by stirring at 1800 rpm for 10 min. Finally, the mixture was ultrasonicated for 30 min at 40 °C. The results reveal that agglomeration of nanoparticles occurred at higher filler loadings, which acted as stress concentration points, leading to a reduction in the mechanical properties of the composites. The authors [47] investigated the time required to fill the die for epoxy composites made by adding glass fiber and alumina nanoparticles. They found that the filling time increased when the filler loading reached 3%, which was due to the increased fluid viscosity and greater resistance provided by the resin-filler mixture to the vacuum pressure. Hongxia Wang used the resin transfer molding technique to prepare epoxy (EP) composites using graphene oxide and reduced graphene oxide (GO) as reinforcements. The properties of GO/EP composites, such as glass transition temperature (Tg), hardness, and nanoindentation depth, decreased by 20.32%, 16.00%, and 416.3 nm, respectively, after γ-ray irradiation compared to standard epoxy composites. The improvement in mechanical properties and thermal stability of the composites was attributed to graphene nanoparticles, which reduced the free radicals responsible for damaging the crosslinked epoxy network [48].

In the case of thermoplastic composites, melt compounding was performed by mixing GNPs into the PP melt using mechanical equipment, a cost-effective, efficient, and eco-friendly method suitable for industrial production. However, poor interface compatibility between graphene and nonpolar polymers like polyolefins can hinder the even distribution of GNPs. PP, a widely used polyolefin, is favored for its balanced mechanical properties, ease of processing and molding, and low cost [49]. Two common techniques are used to improve GNP dispersion in the PP matrix. The first involves adding a compatibilizer, and the second involves modifying the graphene during production. For example, incorporating PP-g-MA as a compatibilizer has been shown to moderately improve compatibility between GNPs and the PP matrix, resulting in better graphene dispersion [50].

Hybrid composites possess high strength, low weight, ease of construction, low production cost, improved chemical resistance, enhanced thermal stability, and a favorable strength-to-weight ratio. These composites are used in various exterior and interior applications within the automotive industry. PP is one of the major polymers utilized in structural and automotive applications; however, it has lower energy absorption, ultimate tensile strength, and thermal properties. To enhance these characteristics, a polypropylene hybrid composite was prepared using Al-C LDH, GNPs, and $CaCO_3$, along with PP-g-MA.

In this study, we focused on developing PP hybrid composites reinforced with Al-C LDH, $CaCO_3$, and GNPs. LDHs are known for their multifunctional and tunable characteristics, while GNPs offer superior properties compared to carbon nanotubes (CNTs). Using the co-precipitation method, Al-C LDH was synthesized and incorporated into the PP matrix alongside $CaCO_3$ and GNPs to create PP/2$CaCO_3$/2Al-C LDH/GNPs-x wt% (x = 0, 0.5, 1.0, 1.5, and 2.0) hybrid composites. A compatibilizer, PP-g-MA, was added to improve the dispersion of GNPs in the nonpolar PP matrix. The hybrid composites were prepared using injection molding with a twin-screw extruder. The primary aim of the study is to comprehensively investigate the effect of GNPs on the mechanical and thermal properties of PP hybrid composites. The research demonstrates that incorporating 1.5 wt% GNPs leads to a significant improvement in ultimate tensile strength. Additionally, thermogravimetric analysis (TGA) shows enhanced thermal stability with increasing GNP content. The novelty of this study lies in the synergistic effect of Al-C LDH, $CaCO_3$, and GNPs, which together enhance energy absorption and residual velocity. Strong interfacial bonding between the reinforcements and the PP matrix ensures efficient load transfer, resulting in superior mechanical properties. The optimal formulation, PP/$CaCO_3$/Al-C LDH/1.0 GNPs, exhibits the best combination of thermal and mechanical performance, making it suitable for structural and high-end applications.

2. Materials and methods

2.1. Materials

PP, a homopolymer in granule form with a size range of 2.5–3.5 mm, was obtained from SABIC, Saudi Arabia, and used as the base polymer. PP-graft-maleic anhydride (PP-g-MA, NG2002 grade) and $CaCO_3$ were sourced from the local market in Riyadh, Saudi Arabia. Exfoliated GNPs (M-5 grade), with an average diameter of 5 μm and a thickness of 8 nm in dry powder form [51], were supplied by Nanografi, Cankaya/Ankara, Turkey. Aluminum nitrate ($Al(NO_3)_3 \cdot 9H_2O$, $\geqslant$ 99.0%), activated carbon (C), and sodium nitrate ($NaNO_3$) were purchased from Srihari Scientific, Chennai, India.

2.2. Synthesis of aluminum-carbon layered double hydroxide (Al-C LDH)

LDH based on Al and carbon black was synthesized using the co-precipitation method as described in previous studies [30,31]. An aqueous solution was prepared with aluminum nitrate ($Al(NO_3)_3$), carbon black, and sodium nitrate ($NaNO_3$) in a 1:1:1 molar ratio. Sodium hydroxide (NaOH) solution was added dropwise to the mixture while stirring continuously until the pH reached 10. The mixture then underwent a hydrothermal reaction at 120 °C for 15 h. The resulting mixture was washed several times with deionized water and centrifuged. Finally, the processed sample was dried at 80 °C for 2 h. Figure 1 illustrates the methodology involved in the synthesis of Al-C LDH.

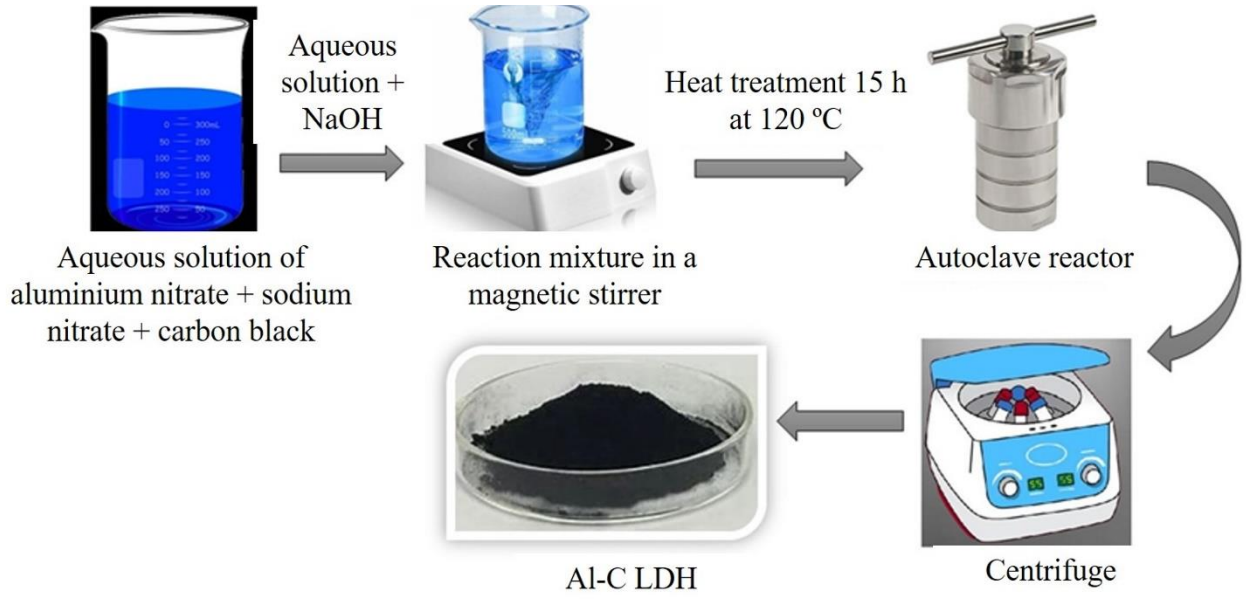

Figure 1. Synthesis of Al-C LDH by co-precipitation method.

2.3. Development of PP/$CaCO_3$/Al-C LDH/GNPs hybrid composite polymers

The PP, PP-g-MA, $CaCO_3$, Al-C LDH, and GNPs were mixed and dried at 80 °C in an oven for up to 1 h to remove moisture and volatile contents. GNPs were loaded in weight percentages of 0, 0.5, 1.0, 1.5, and 2.0, along with 2.0 wt% Al-C LDH and 2.0 wt% $CaCO_3$ in the PP matrix (with 5 wt% PP-g-MA acting as a compatibilizer). Table 1 presents the sample identifications (IDs), compositions, and reinforcement percentages. PP-g-MA and GNPs were dispersed in ethanol at a ratio of 100:15 (ethanol:materials) using a magnetic stirrer for 30 min to minimize GNP agglomeration in the PP matrix, followed by drying at 353 K for 2 h in an oven. All materials were then mechanically blended for approximately 45 min to ensure thorough homogenization.

A twin-screw extruder was used for the simultaneous melting and compounding of the mechanically blended mixture to prepare the hybrid composites. The specifications of the extruder are as follows: screw diameter of 21 mm, 220 V, 1.1 kW power, output range of 100–3000 g/h, production linear speed of <1000 cm/min, and machine dimensions of 1800 × 200 × 1000 mm (Make: M/s Dongguan Junxin Plastic & Metal Co. Ltd., Qiaotou Town, Dongguan, China), as discussed in our previous research [51]. Figure 2 illustrates the compounding of PP, PP-g-MA, $CaCO_3$, Al-C LDH, and

GNPs using the twin-screw extrusion process, followed by a vertical injection molding machine used to create the test specimens.

Table 1. Sample designation, sample ID, percentage of PP, GNPs, Al C LDH, $CaCO_3$, and PP-g-MA.

Sample designation	Sample ID	PP (wt%)	GNP (wt%)	Al-C LDH (wt%)	$CaCO_3$ (wt%)	PP-g-MA (wt%)
PP	Neat PP	100	-	-	-	-
PP + 2$CaCO_3$ + 5PP-g-MA + 2Al C LDH + 0.5GNP	PP/$CaCO_3$/LDH/0.5GNPs	92.5	0.5	2	2	5
PP + 2$CaCO_3$ + 5PP-g-MA + 2Al C LDH + 1GNP	PP/$CaCO_3$/LDH/1.0GNPs	92	1	2	2	5
PP + 2$CaCO_3$ + 5PP-g-MA + 2Al C LDH + 1.5GNP	PP/$CaCO_3$/LDH/1.5GNPs	91.5	1.5	2	2	5
PP + 2$CaCO_3$ + 5PP-g-MA + 2Al C LDH + 2GNP	PP/$CaCO_3$/LDH/2.0GNPs	91	2	2	2	5

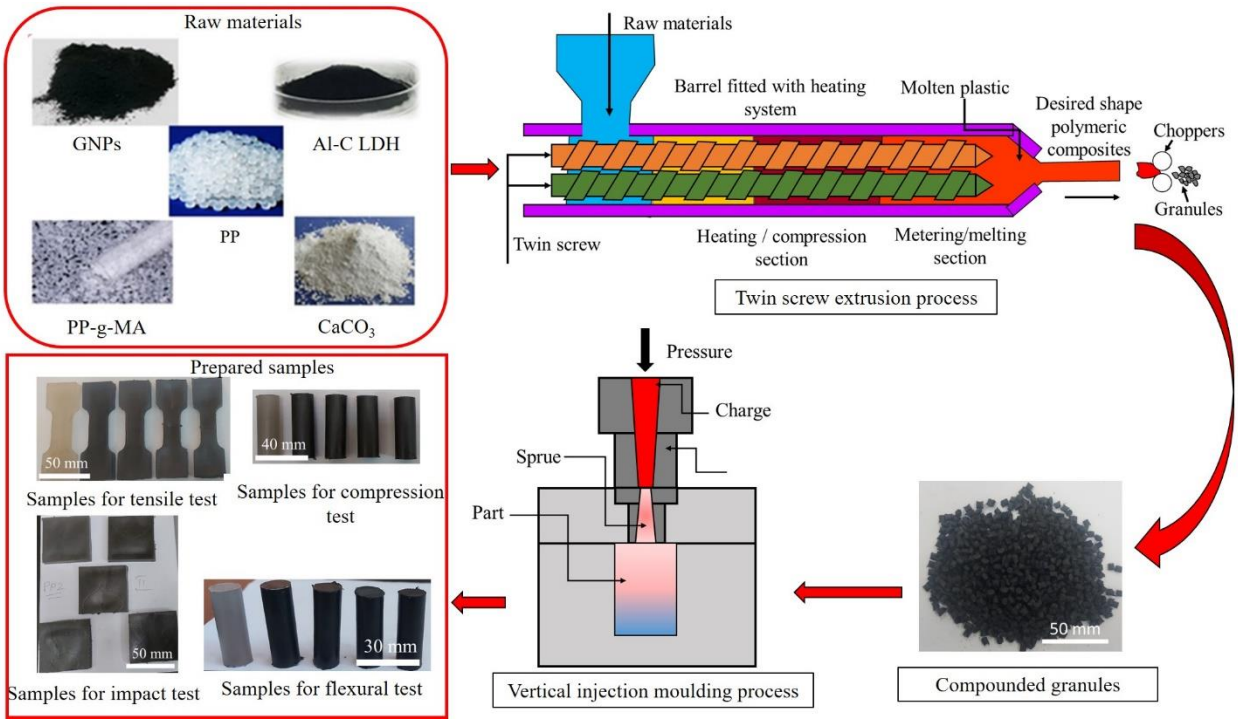

Figure 2. Schematic diagram representing the compounding of PP, PP-g-MA, $CaCO_3$, Al-C LDH, and GNPs hybrid composite polymers using twin extrusion followed by vertical injection molding for fabrication of parts.

2.4. Characterization of developed PP/$CaCO_3$/Al-C LDH/GNPs hybrid composite polymers

2.4.1. FEG-HRSEM

FEG-HRSEM was used to evaluate the surface characteristics of the synthesized Al-LDH, neat PP, PP/$CaCO_3$/LDH/1.0 GNPs, and PP/$CaCO_3$/LDH/2.0 GNPs hybrid polymer composite samples. This technique was also employed to investigate the fracture surfaces of samples subjected to mechanical testing, including tensile and impact tests. An Apreo FEG-HRSEM instrument was utilized, operating at a voltage of 30 keV with a resolution of 1.3 nm.

2.4.2. X-ray diffraction (XRD)

XRD analysis was performed on neat PP, PP/$CaCO_3$/LDH/1.0 GNPs, and PP/$CaCO_3$/LDH/2.0 GNPs hybrid polymer composite samples to identify the different phases present. The examination was conducted using a PANalytical X'Pert Pro instrument with Cu-Kα radiation. Samples were scanned at diffraction angles ranging from 5 to 90° at a scanning speed of 2°/min. The resulting peak data were analyzed using the X'pert High Score Plus software.

2.4.3. X-ray photoelectron spectroscopy (XPS)

XPS analysis (M/s Thermo Fisher) was performed on the selected samples (neat PP, PP/$CaCO_3$/LDH/1.0 GNPs, and PP/$CaCO_3$/LDH/2.0 GNPs). This analysis aimed to investigate the elemental composition, chemical properties, and overall structure of the developed polymers. XPS is a robust and reliable characterization method for revealing the bonding characteristics of the incorporated elements.

2.4.4. Fourier-transform infrared spectroscopy (FTIR)

FTIR testing (ASTM E168-16 standard) [52] was conducted on the neat PP, PP/$CaCO_3$/LDH/1.0 GNPs, and PP/$CaCO_3$/LDH/2.0 GNPs samples to identify the chemical compounds present in the developed composite polymers. The tests were performed using a JASCO BSA spectrometer with a resolution of 4 cm^{-1} over a wavelength range of 4000 to 380 cm^{-1}. This FTIR instrument provides high-spectral infrared data, which is then processed using Fourier transform. This transformation enables the identification of chemical compounds, crystalline properties, and any unidentified phases present in the samples.

2.4.5. TGA

TGA was performed on the developed samples using a TA instrument (New Castle, DE, USA). In this analysis, each sample was heated from 25 to 700 °C at a rate of 10 °C/min, with all tests conducted in a nitrogen atmosphere. Key TGA parameters include the onset temperature, which indicates the temperature at which initial weight loss begins.

2.4.6. Nanoindentation test

The nanoindentation test was performed on hybrid composites fabricated with a PP matrix containing GNPs at varying weight percentages (0.5, 1.0, 1.5, and 2.0), along with 2 wt% Al-C LDH, 2 wt% $CaCO_3$, and 5 wt% PP-g-MA. Measurements were taken using a Berkovich diamond indenter with a 500 nm tip radius. The test employed a dwell duration of 5 s and a maximum constant load of 10 mN, with an average of five readings obtained for each sample. The indentation load-depth profile was analyzed using the Oliver and Pharr method.

2.5. Mechanical testing of tensile, compression, 3P bending, and low-velocity impact tests

Tensile tests were conducted according to ASTM D638 using an MTS universal testing machine (model No: 370.25, 250 kN capacity) to determine the mechanical properties, including yield strength, ultimate strength, and elongation at rupture. A loading rate of 1 mm/min was applied during the tests, and an average of five trials for each composition was used for interpretation. Flexural testing was performed according to ASTM D790 using the same MTS universal testing apparatus with a specific attachment. The samples had a span of 40 mm between supports, with the load applied at the center during the flexural tests. Uniaxial compression tests were conducted per ASTM D695 to assess the compressive strengths of the developed samples. The samples had a diameter of 15 mm and a length of 22.5 mm, with at least five trials performed for each composition. Additionally, low-velocity impact tests (LVI) were conducted according to ASTM D7136 on 60 mm square samples with a thickness of 10 mm.

3. Results and discussion

3.1. FEG-HRSEM analyses of PP/$CaCO_3$/Al-C LDH/ x wt% GNPs hybrid composites

The surface morphology and chemical composition of the synthesized Al-C LDH powder were investigated using FEG-HRSEM, as shown in Figure 3a,b. Figure 3a displays the equiaxed, flower-like-shaped powders (C) and polygonal-shaped powders (Al) observed in Al-C LDHs. Additionally, the corresponding EDX spectra in Figure 3b exhibit strong Al and C peaks, confirming the successful synthesis of Al-C LDHs. The EDX results indicate that the atomic weight percentages of Al and C are 12.66% and 46.03%, respectively, validating the formation of Al-C LDH. The surface morphology of the as-received GNP powder, shown in Figure 3c,d, reveals a flake-like layered structure with a thickness of approximately 10 nm.

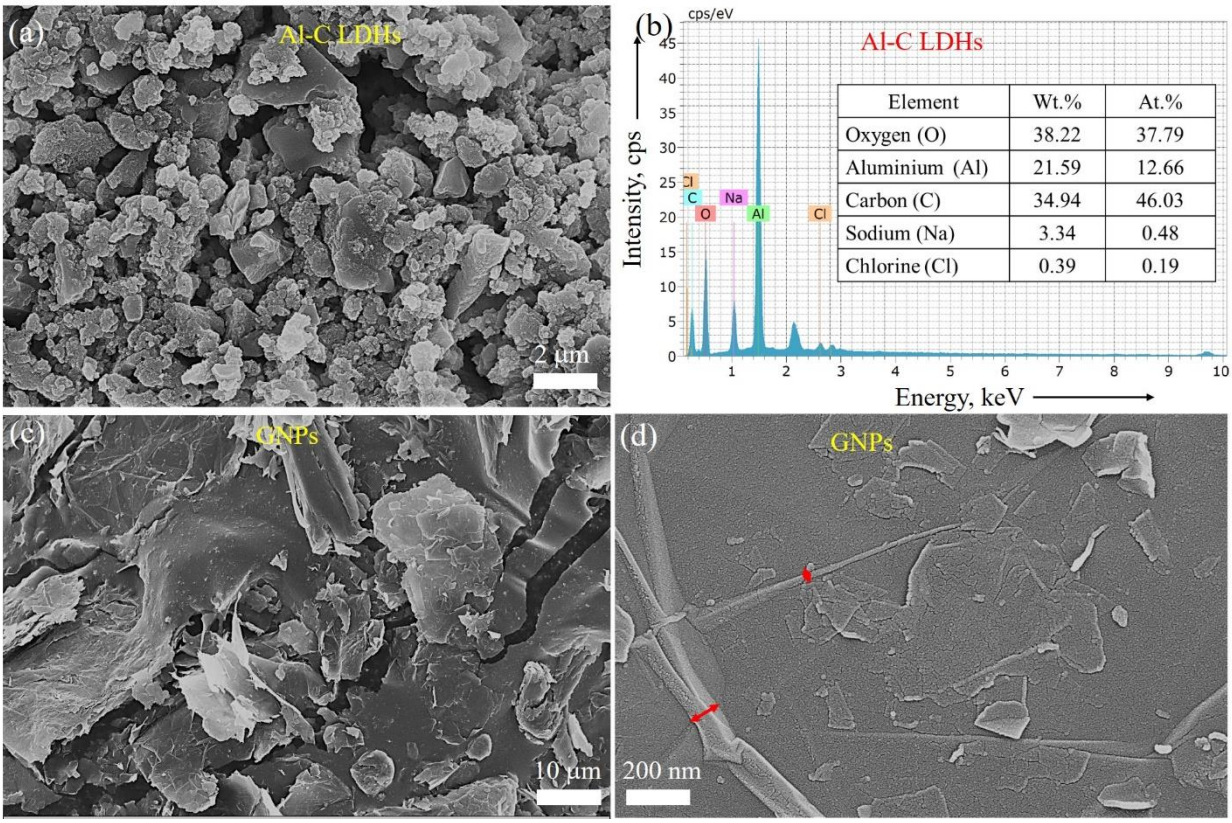

Figure 3. HRSEM analyses of synthesized Al-C LDH and as-received GNPs: (a) SEM morphology of Al-C LDHs; (b) corresponding EDAX spectra with composition (inset) of Al-C LDHs; (c, d) SEM morphology of as-received GNPs. The red arrow in (d) indicates the thickness of GNPs.

Figure 4 presents the HRSEM images of neat PP and various GNP loadings (0.5, 1, 1.5, and 2 wt%) in $CaCO_3$/Al-C LDH/GNPs hybrid composites. The dispersion of GNPs, $CaCO_3$, and Al-C LDH particles is evident in all hybrid composites. As the GNP loading increased from 0.5 to 2 wt%, agglomeration within the PP/$CaCO_3$/Al-C LDH/GNPs composites also increased due to inadequate dispersion beyond a certain threshold. It was observed that the $CaCO_3$/Al-C LDH/2.0 GNPs hybrid composites (Figure 4i,j) exhibited an uneven distribution of GNPs. The higher loading of 2 wt% GNPs, along with $CaCO_3$ and Al-C LDH, led to poor dispersion and is expected to decrease the mechanical properties compared to pure PP (Figure 4a,b). Figure 4c–e represent 0.5 wt% and 1 wt% of GNPs in the PP/$CaCO_3$/Al-C LDH/GNPs hybrid composite polymer, respectively. These results show that the reinforcement of GNPs and Al-C LDH nanoparticles is uniformly dispersed in the PP matrix. Figure 5a–f presents HRSEM-BSE elemental mapping and EDS analyses of the PP/$CaCO_3$/Al-C LDH/1.0 GNPs hybrid composite polymer, with insets showing the detected elemental composition. The images illustrate the microstructure (Figure 5a) and the presence of carbon (C) (Figure 5b), calcium (Ca) (Figure 5c), oxygen (O) (Figure 5d), and aluminum (Al) (Figure 5e) within the hybrid composites (Figure 5f). This confirms the successful incorporation of compatibilizers, GNPs, and Al-C LDH into the polymer matrix during processing.

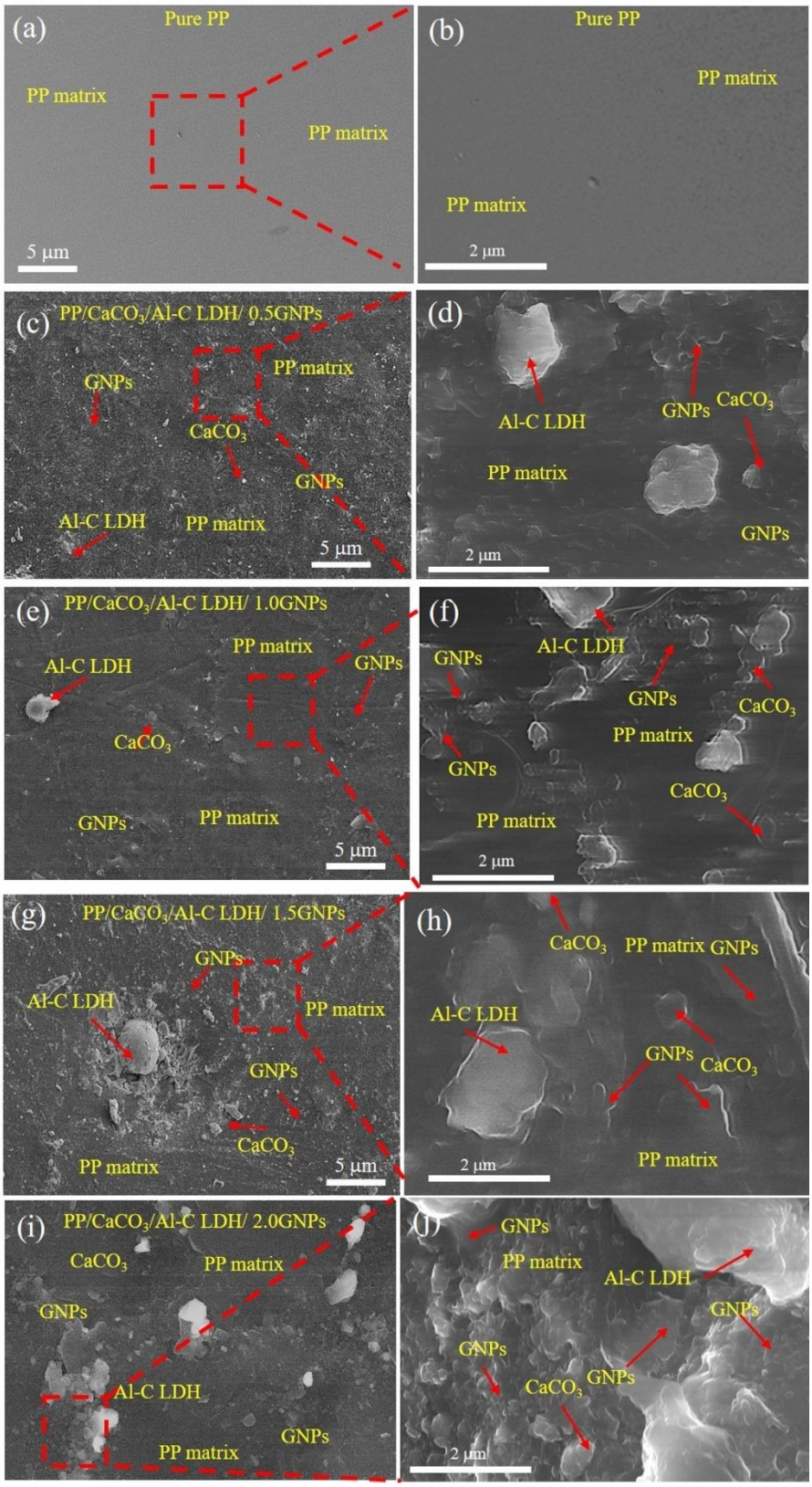

Figure 4. HRSEM analyses of injection molded specimen of (a, b) neat PP; (c, d) PP/$CaCO_3$/Al-C LDH/0.5 GNPs; (e, f) PP/$CaCO_3$/Al-C LDH/1.0 GNPs; (g, h) PP/$CaCO_3$/Al-C LDH/1.5 GNPs; (i, j) PP/$CaCO_3$/Al-C LDH/2.0 GNPs hybrid composites.

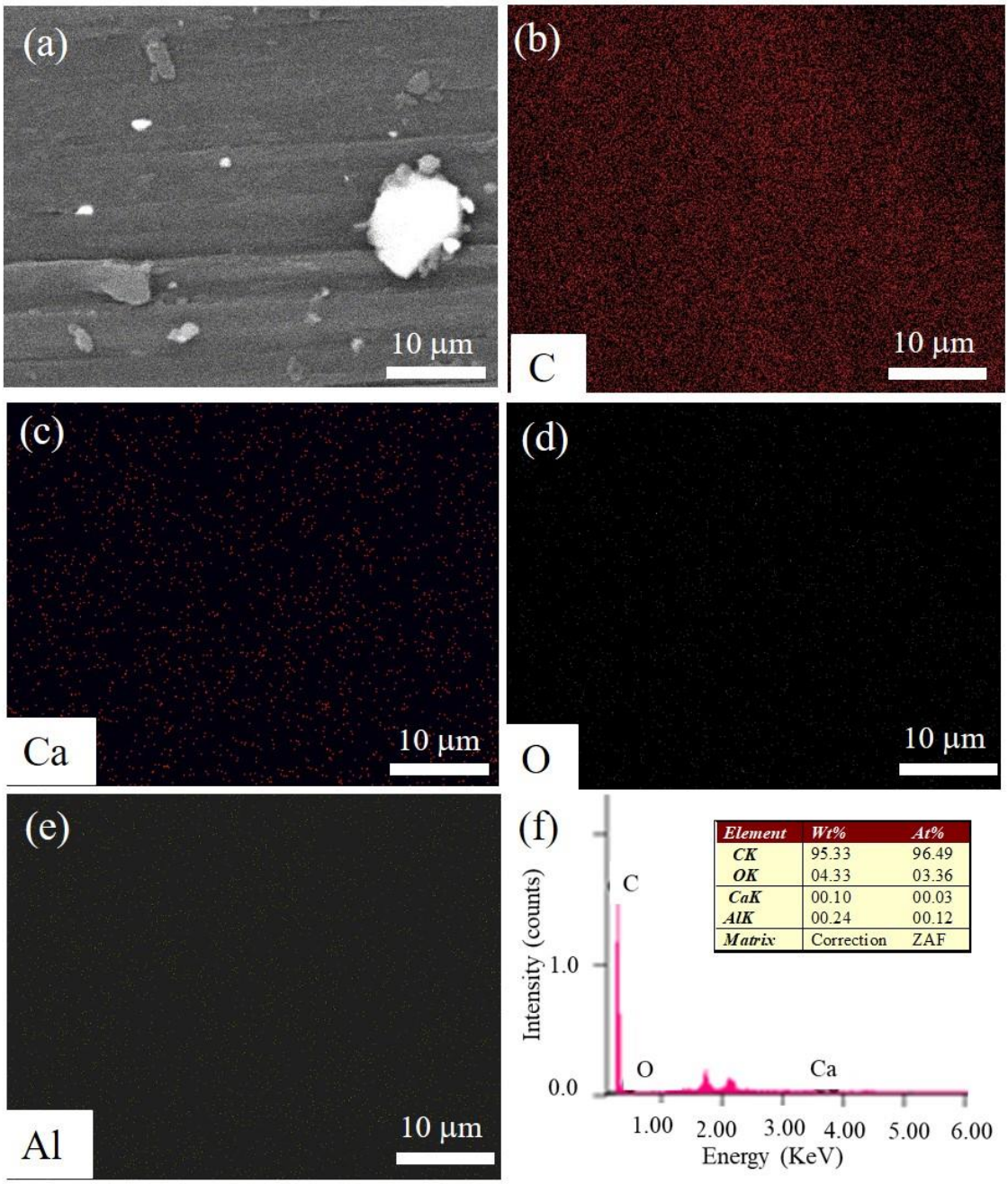

Figure 5. HRSEM-BSE elemental mapping of PP/$CaCO_3$/Al-C LDH/1.0 GNPs hybrid composites: (a) microstructure; (b) C; (c) Ca; (d) O; (e) Al; and (f) EDS result of (a).

3.2. XRD analyses on developed hybrid composite polymers

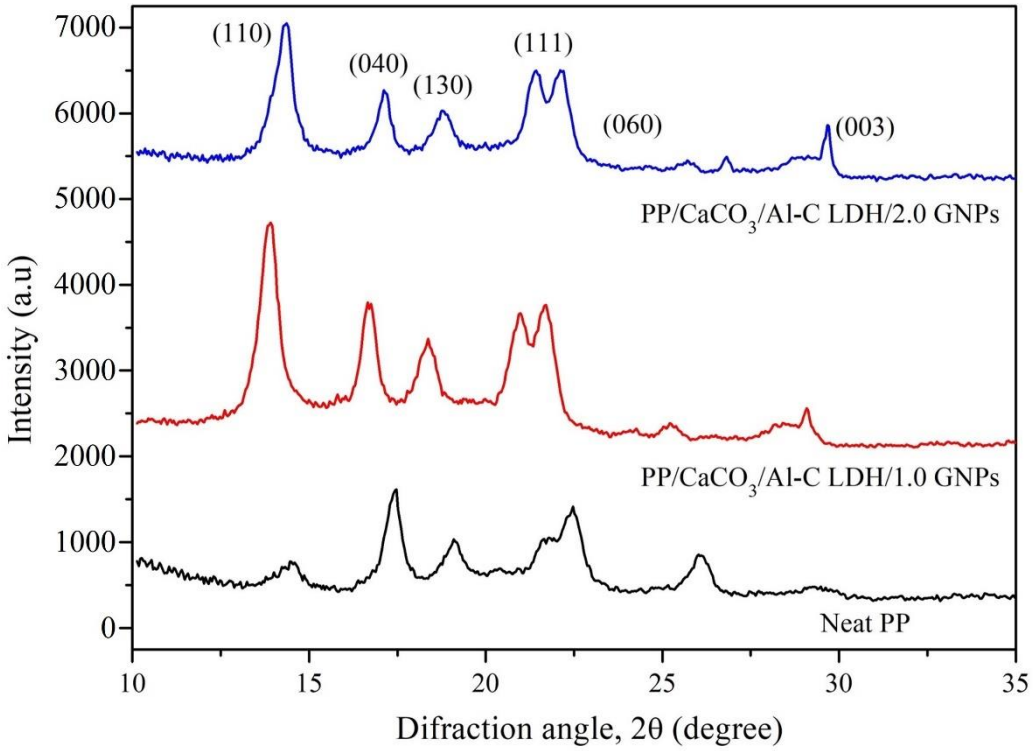

Figure 6. XRD peak profiles of developed neat PP, PP/$CaCO_3$/Al-C LDH/1.0 GNPs, and PP/$CaCO_3$/Al-C LDH/2.0 GNPs hybrid composite polymers obtained from extrusion.

Figure 6 illustrates the XRD peak profiles of neat PP, PP/$CaCO_3$/Al-C LDH/1.0 GNPs, and PP/$CaCO_3$/Al-C LDH/2.0 GNPs hybrid composites. The neat PP matrix exhibited XRD peaks at 2θ angles of 14.1, 17.1, 18.6, 22.6, 25.4, and 31.0°, corresponding to the (110), (040), (130), (111), (060), and (003) planes, respectively. The inclusion of $CaCO_3$, Al-C LDH, and GNPs in the hybrid composites was evidenced by XRD profiles at 2θ angles of 26.4 and 26.8°, associated with the (104), (003), and (002) planes. The results indicate that the addition of ultra-fine GNPs broadened and reduced the intensity of the PP matrix peaks. Furthermore, the peak related to GNPs increased in intensity with higher GNP content, suggesting successful composite formation. An increase in GNP loading caused a shift in the peak positions of the α-form PP matrix, attributed to the significant interfacial tension between the incorporated GNPs and the PP matrix, as evidenced by the XRD characteristics of the hybrid composites at 2θ angles of 26.4 and 26.8°. This significant interfacial tension results from the increased viscosity of the PP matrix with GNP inclusion. According to [53] and [54], the β-form of PP crystals can be moderated by the addition of a PP-MAH compatibilizer to the PP matrix. Consequently, no β-form PP crystals were observed in the current XRD results.

3.3. XPS analysis

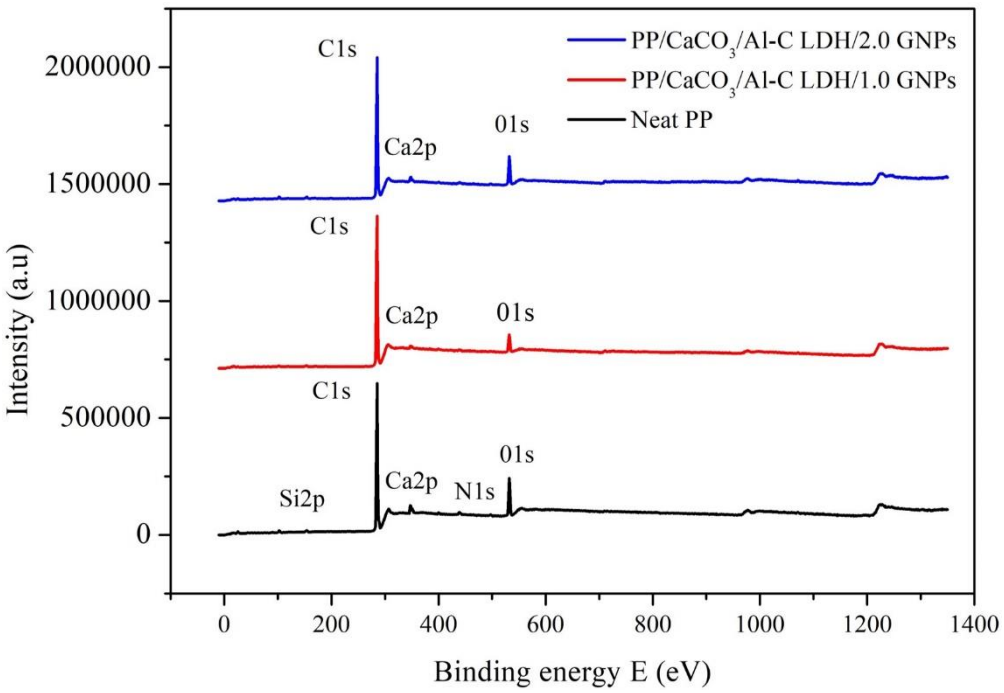

Figure 7. XPS of developed neat PP, PP/$CaCO_3$/Al-C LDH/1.0 GNPs, and PP/$CaCO_3$/Al-C LDH/2.0 GNPs hybrid composite polymers obtained from extrusion.

Table 2. Chemical composition of different elements in the developed neat PP matrix, PP/$CaCO_3$/Al-C LDH/1.0 GNPs, and PP/$CaCO_3$/Al-C LDH/2.0 GNPs hybrid composite polymers measured using XPS.

Name of sample	Atomic concentrations (%)				
	C1s	O1s	Ca2p	Al2p	Al2s
Neat PP	86.89	13.11	-		
PP/$CaCO_3$/Al-C LDH/1.0 GNPs	87.39	9.83	1.15	0.88	0.75
PP/$CaCO_3$/Al-C LDH/2.0 GNPs	91.58	6.85	0.68	0.65	0.24

Figure 7 shows the XPS profiles of neat PP, PP/$CaCO_3$/Al-C LDH/1.0 GNPs, and PP/$CaCO_3$/Al-C LDH/2.0 GNPs hybrid composites, illustrating their chemical composition. Table 2 details the atomic percentages of the observed elements from the developed PP/$CaCO_3$/Al-C LDH/x wt% GNPs hybrid composite polymers. The successful formation of composites is evidenced by the increased C1s peak intensity with rising GNP content (0–2 wt%) and the presence of Al2p, Al2s, Ca2p, and Si2p, as indicated by the XPS analysis (Figure 7). Conversely, the O1s peak intensity decreased with increasing GNP content, suggesting proper bonding and nucleation of GNPs within the PP matrix [51,55]. The increase in C content with the addition of GNPs (Table 2) can be attributed to several factors, including the surface chemistry of GNPs, aggregation of GNPs, XPS sensitivity and depth detection (1–10 nm), and interfacial interaction between the PP matrix and GNPs, which produced the nonlinear relationship observed in the XPS data. Typically, GNPs possess a high surface area that may contain several

functional groups. As GNP loading increased to 1%, the surface area available for interaction with the PP matrix was expected to increase, resulting in a rise in the carbon signal. However, when the GNP loading was increased to 2%, the formation of GNP agglomeration and a higher concentration of carbon atoms in the surface area of the PP/$CaCO_3$/Al-C LDH/2.0 GNPs hybrid composites was anticipated to produce a disproportionate increase in carbon detection.

3.4. FTIR analysis

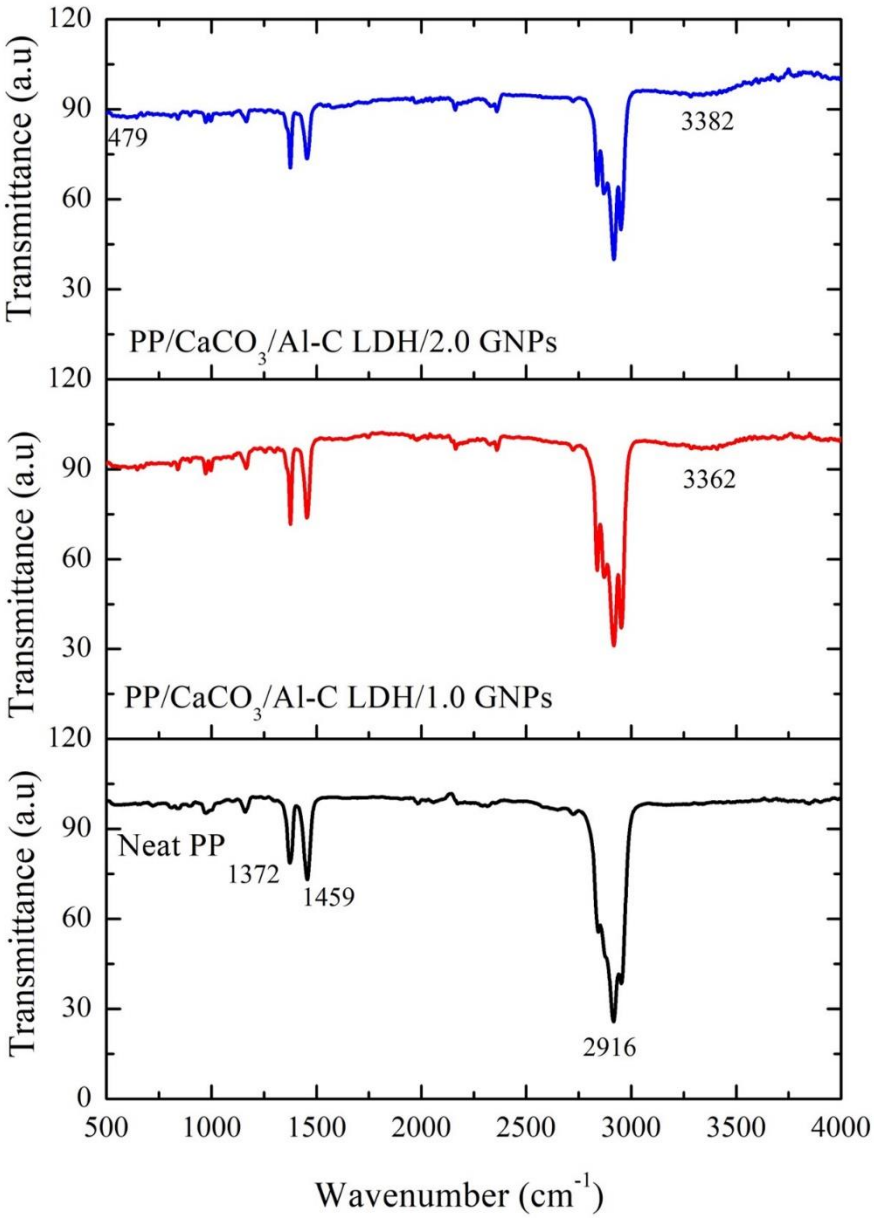

Figure 8. FTIR profile of developed neat PP, PP/$CaCO_3$/Al-C LDH/1.0 GNPs, and PP/$CaCO_3$/Al-C LDH/2.0 GNPs hybrid composites polymers.

FTIR was conducted in the wavelength range of 4000 to 400 cm^{-1} using a JASCO BSA spectrometer with a resolution of 4 cm^{-1}. FTIR testing was performed on neat PP, PP/$CaCO_3$/Al-C

LDH/1.0 GNPs, and PP/$CaCO_3$/Al-C LDH/2.0 GNPs hybrid composites to determine the presence of chemical compounds in the developed materials. The molecular bond formation and stretching vibrations of neat PP, PP/$CaCO_3$/Al-C LDH/1.0 GNPs, and PP/$CaCO_3$/Al-C LDH/2.0 GNPs were examined using FTIR, with the corresponding profiles shown in Figure 8. Peaks at 1459 and 1372 cm^{-1} were assigned to $–CH_3$ and $–CH_2$ groups, while the peak at 2916 cm^{-1} corresponded to the $–C–CH_2–C–$ stretching vibration of polypropylene. Small characteristic peaks at 955 and 964 cm^{-1} were attributed to C–C stretching and CH_3 asymmetric rocking, with a peak at 829 cm^{-1} corresponding to C–H rocking in polypropylene [56,57]. The GNPs peak at 2916 cm^{-1} was assigned to the symmetric and asymmetric vibrations of $–CH_2–$, while the peak at 1459 cm^{-1} corresponded to the C=C skeletal bond in the aromatic domain. The OH groups observed at 3362 and 3382 cm^{-1} were due to the O–H stretching vibrations of adsorbed water molecules and structural OH groups [49,58]. Peaks with intensities at 479 and 489 cm^{-1} were attributed to the vibrational modes of the metal-oxygen bond in the layered LDH, characteristic of brucite-like materials [57]. Peaks at 845, 1094, 1455, and 1635 cm^{-1} were attributed to carbonate ions present in $CaCO_3$, with the peak at 1085 cm^{-1} representing the symmetrical stretching and wagging of $(CO_3)^{2-}$.

3.5. TGA of PP/$CaCO_3$/Al-C LDH/GNPs hybrid composites

TGA was performed using a TA Discovery Series instrument from TA (New Castle, DE, USA). Samples were heated from room temperature to 700 °C at a rate of 10 °C/min under a nitrogen atmosphere. The onset temperature, representing the initial weight loss temperature, was derived from the TGA data. Thermal degradation studies were conducted on neat PP, PP/$CaCO_3$/Al-C LDH/1.0 GNPs, and PP/$CaCO_3$/Al-C LDH/2.0 GNPs hybrid composites. The thermal degradation temperatures at various weight loss percentages (5%, 10%, 20%, and 50%) and the residue percentage at 500 °C are listed in Table 3. The incorporation of LDHs (2% Al-C LDH) along with GNPs improved thermal stability compared to neat PP, due to the strong nucleating and bonding effects of GNPs within the PP matrix, as shown in Figure 9 and Table 3. GNPs prevent the evaporation of volatiles, and their large surface area absorbs free radicals generated during thermal decomposition [56,57]. The initial degradation temperatures (T5%, T10%, T20%, and T50%) for neat PP were 371.89, 406.49, 433.99, and 460.35 °C, respectively. In contrast, for the PP/$CaCO_3$/Al-C LDH/2.0 GNPs hybrid composite, the corresponding temperatures were 417.41, 441.73, 458.51, and 472.06 °C, respectively. The good compatibility of Al-C LDH with GNPs in PP improved thermal stability from the onset of degradation to the maximum weight loss percentage. The PP/$CaCO_3$/Al-C LDH/2.0 GNPs hybrid composite showed a higher residue percentage of 4.67% compared to neat PP, indicating that the presence of Al-C LDH forms a carbonaceous protective char layer over the PP substrate [49,58].

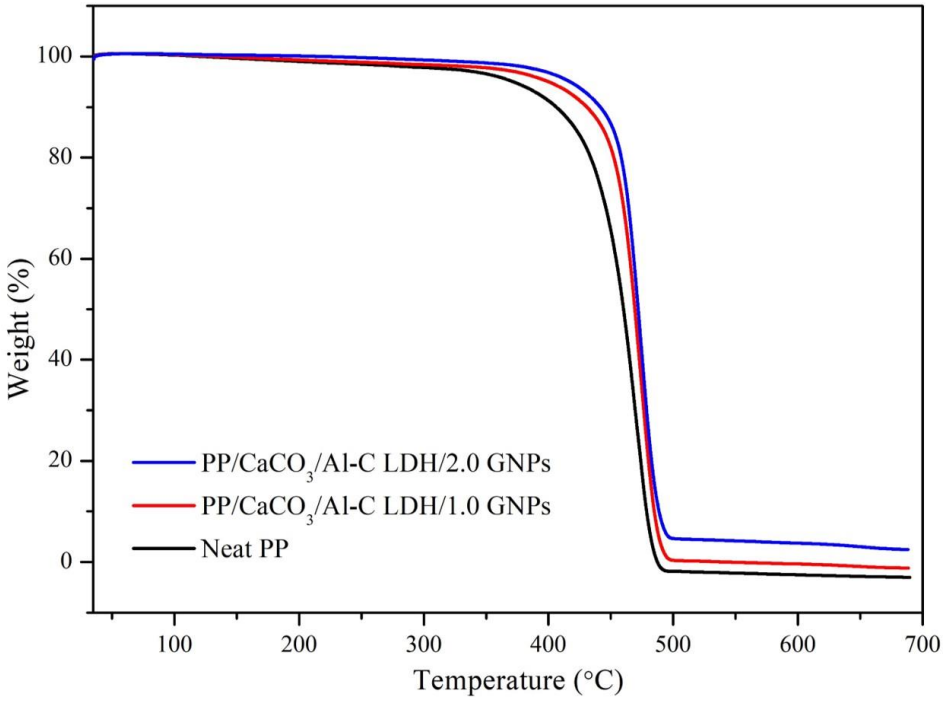

Figure 9. TGA of developed neat PP, PP/$CaCO_3$/Al-C LDH/1.0 GNPs, and PP/$CaCO_3$/Al-C LDH/2.0 GNPs hybrid composite polymers.

Table 3. TGA of developed neat PP, PP/$CaCO_3$/Al-C LDH/1.0 GNPs, and PP/$CaCO_3$/Al-C LDH/2.0 GNPs hybrid composites.

Name of sample	Thermal degradation temperature (°C)				Residue percentage at 500 °C
	Weight loss at 5%, T_5 (°C)	Weight loss at 10%, T_{10} (°C)	Weight loss at 20%, T_{20} (°C)	Weight loss at 50%, T_{50} (°C)	
Neat PP	371.89	406.49	433.99	460.35	0
PP/$CaCO_3$/Al-C LDH/1.0 GNPs	400.13	430.94	452.56	469.42	0.30
PP/$CaCO_3$/Al-C LDH/2.0 GNPs	417.41	441.73	458.51	472.06	4.67

3.6. Examination of mechanical properties of developed PP/$CaCO_3$/Al-C LDH/x wt% GNPs hybrid composite polymers

3.6.1. Tensile stress-strain behavior

Figure 10 shows the mechanical properties of neat PP, PP/$CaCO_3$/Al-C LDH/0.5 GNPs, PP/$CaCO_3$/Al-C LDH/1.0 GNPs, PP/$CaCO_3$/Al-C LDH/1.5 GNPs, and PP/$CaCO_3$/Al-C LDH/2.0 GNPs hybrid composites. Compared to pure PP, the tensile strength began to increase with the addition of GNPs (up to 1.5 wt%), after which it started to decrease with the addition of 2 wt% GNPs. Similarly, as the percentage of GNPs increased up to 1.5%, the modulus of elasticity gradually increased but then decreased at 2.0% GNPs. Figure 10 and Table 4 provide detailed mechanical properties of the

developed hybrid composites. The results clearly indicate that as the fraction of GNPs with Al-C LDH increases, the tensile strength of the pure PP matrix also increases significantly. For example, the tensile strengths were measured as follows: 35.829 MPa for pure PP, 40.84 MPa for PP/$CaCO_3$/Al-C LDH/0.5 GNPs, 42.24 MPa for PP/$CaCO_3$/Al-C LDH/1.0 GNPs, 44.85 MPa for PP/$CaCO_3$/Al-C LDH/1.5 GNPs, and 44.11 MPa for PP/$CaCO_3$/Al-C LDH/2.0 GNPs. The tensile strength dropped when 2 wt% GNPs were added. The enhanced tensile strength for the hybrid composite polymers of PP/$CaCO_3$/Al-C LDH/0.5 GNPs, PP/$CaCO_3$/Al-C LDH/1.0 GNPs, PP/$CaCO_3$/Al-C LDH/1.5 GNPs, and PP/$CaCO_3$/Al-C LDH/2.0 GNPs was found to be 13.98%, 18.74%, 25.17%, and 23.11% higher than that of the pure PP matrix, respectively. This improvement is attributed to the effective load transfer between the PP matrix and GNP fillers, facilitated by the nucleating impact of GNPs in the PP matrix, appropriate bonding of the inserted GNPs with Al-C LDH, and uniform dispersion of GNPs/Al-C LDH. GNPs possess high stiffness, which contributes to enhancing the rigidity of the composite matrix. It was observed that the incorporated GNPs, up to 1.5 wt%, were effectively dispersed within the PP matrix (see Figure 4a,b), which is expected to improve load transfer between the PP matrix and the $CaCO_3$/Al-C LDH/GNPs hybrid reinforcements. This resulted in enhanced mechanical properties, including the modulus of elasticity. However, as the GNP content increased beyond 1.5 wt%, a decrease in the mechanical properties, including the modulus of elasticity, was noted. This decline can be attributed to the agglomeration of GNPs (see Figure 4i,j) and improper dispersion within the PP matrix. Such agglomeration weakens the load transfer rate and decreases the effective interface area between the $CaCO_3$/Al-C LDH/GNPs and the PP matrix. Consequently, the modulus of elasticity decreases with increasing GNP content.

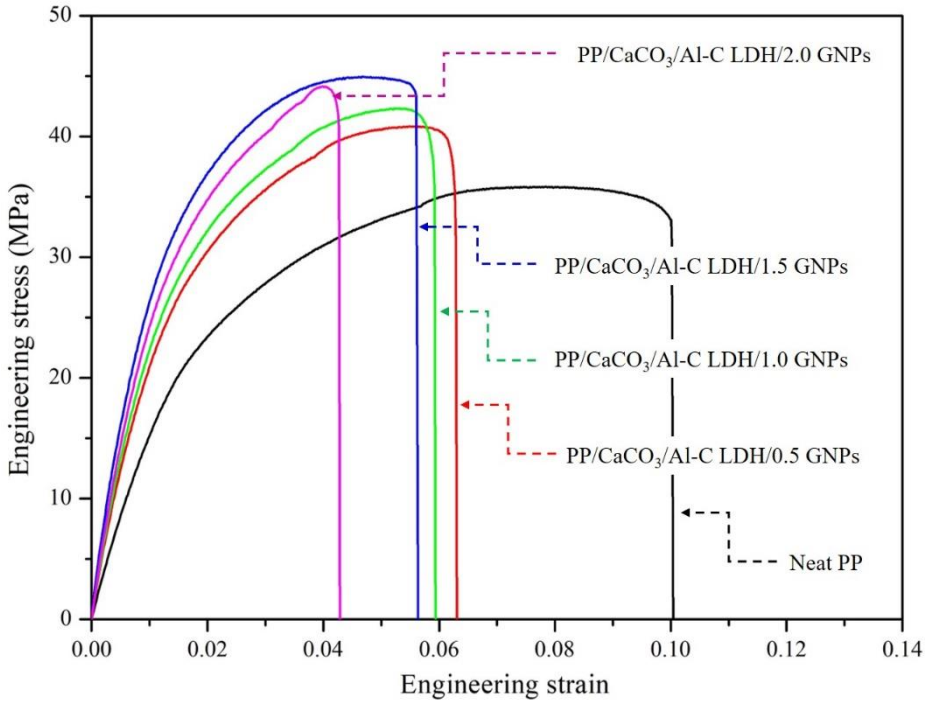

Figure 10. Engineering stress-strain curves of neat PP, PP/$CaCO_3$/Al-C LDH/0.5 GNPs, PP/$CaCO_3$/Al-C LDH/1.0 GNPs, PP/$CaCO_3$/Al-C LDH/1.5 GNPs, and PP/$CaCO_3$/Al-C LDH/2.0 GNPs hybrid composite polymers obtained from the uniaxial tensile test.

Table 4. Mechanical properties of newly developed neat PP, PP/$CaCO_3$/Al-C LDH/0.5 GNPs, PP/$CaCO_3$/Al-C LDH/1.0 GNPs, PP/$CaCO_3$/Al-C LDH/1.5 GNPs, and PP/$CaCO_3$/Al-C LDH/2.0 GNPs hybrid composite polymers obtained from the uniaxial tensile test.

Sample ID	Modulus of elasticity (MPa)	Tensile yield stress (MPa)	Tensile strain at yield point	Ultimate tensile stress (MPa)	Tensile strain at ultimate point
Neat PP	1921.869 ± 36.58	20.896 ± 0.65	0.016 ± 0.0021	35.829 ± 0.38	0.078 ± 0.0011
PP/$CaCO_3$/Al-C LDH/0.5 GNPs	2995.059 ± 32.65	25.327 ± 0.34	0.013 ± 0.0016	40.838 ± 0.42	0.056 ± 0.0020
PP/$CaCO_3$/Al-C LDH/1.0 GNPs	3091.567 ± 26.85	26.875 ± 0.42	0.014 ± 0.0011	42.244 ± 0.44	0.055 ± 0.0014
PP/$CaCO_3$/Al-C LDH/1.5 GNPs	3891.186 ± 34.65	28.699 ± 0.25	0.020 ± 0.0008	44.849 ± 0.52	0.048 ± 0.0013
PP/$CaCO_3$/Al-C LDH/2.0 GNPs	3385.627 ± 41.32	30.256 ± 0.51	0.019 ± 0.0014	44.110 ± 0.22	0.041 ± 0.0016

In addition, it was observed that the incorporation of Al-C LDH improved the mechanical properties compared to the PP/$CaCO_3$/x wt% GNPs hybrid composite reported in our previous work [51]. For instance, the highest tensile strength obtained in the PP/$CaCO_3$/1.5 GNPs hybrid composite sample (without Al-C LDH) was 40.55 MPa [51], whereas the PP/$CaCO_3$/Al-C LDH/1.5 GNPs hybrid composite sample produced 44.85 MPa, which is 10.64% higher than the sample without Al-C LDH in the same composition. This improvement is attributed to the effective bonding and dispersion-strengthening effects of the introduced Al-C LDH. These results further confirm the enhancement of mechanical properties with the addition of Al-C LDH to the PP matrix. Figure 11 shows that the tensile strain at the ultimate point significantly decreases as the GNP content in the PP matrix increases. This decrease is due to the rise in defects caused by the introduction of GNPs, $CaCO_3$, and Al-C LDH. Specifically, the tensile strain reduction percentages for the hybrid composite polymers compared to the pure PP matrix were 28.20%, 29.48%, 38.46%, and 47.43% for PP/$CaCO_3$/Al-C LDH/0.5 GNPs, PP/$CaCO_3$/Al-C LDH/1.0 GNPs, PP/$CaCO_3$/Al-C LDH/1.5 GNPs, and PP/$CaCO_3$/Al-C LDH/2.0 GNPs, respectively. This indicates a notable drop in elongation and ductility, suggesting that the increased GNP content hinders chain mobility within the polymer matrix. Consequently, this leads to increased stiffness in the composites, consistent with findings reported in the literature [58,59].

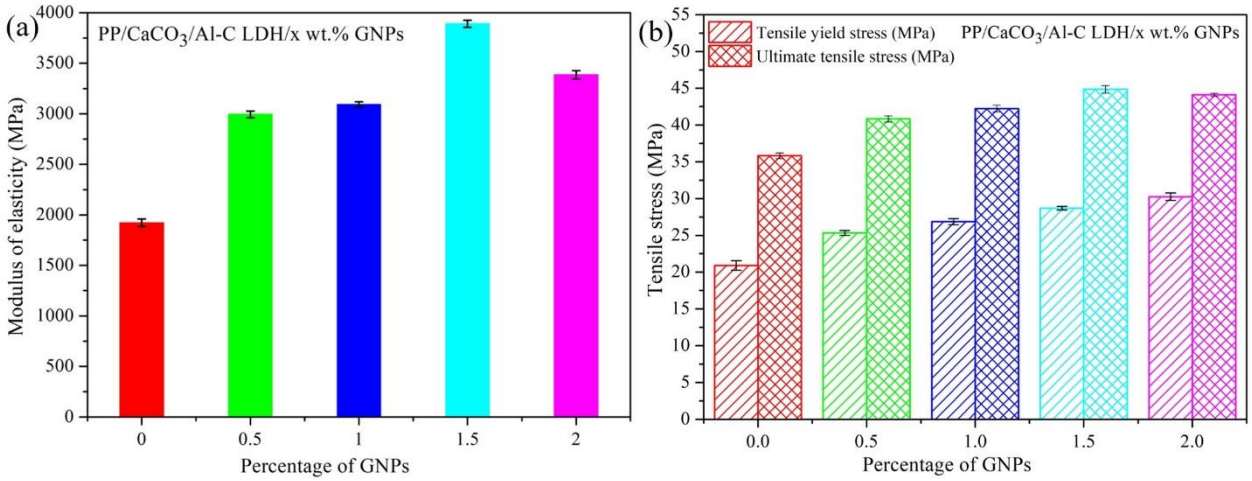

Figure 11. Mechanical properties: (a) modulus of elasticity, (b) tensile yield stress and ultimate tensile stress of developed pure PP matrix, PP/$CaCO_3$/Al-C LDH/0.5 GNPs, PP/$CaCO_3$/Al-C LDH/1.0 GNPs, PP/$CaCO_3$/Al-C LDH/1.5 GNPs, and PP/$CaCO_3$/Al-C LDH/2.0 GNPs hybrid composites.

3.6.2. Compression stress-strain behavior

The compressive properties of the developed PP/$CaCO_3$/Al-C LDH/x wt% GNPs hybrid composite were tested in terms of compressive yield strength, strain at the yield point, ultimate compressive strength, and strain. These properties were obtained from the compressive stress-strain curves, as shown in Figure 12 and Table 5. The stress-strain curves of the hybrid composites exhibit a linear shape; at low strain rates, a high slope is observed under the applied load due to elastic deformation, which is followed by plastic deformation, where the polymeric material yields and permanent deformation occurs due to energy absorption by the reinforcements [60].

The results clearly indicate that the compressive strength of the hybrid composite polymers significantly increases with the addition of GNPs and Al-C LDH to the PP matrix. For instance, the ultimate compressive strength (Figure 13) of the developed hybrid composite polymers improved by 21.59%, 27.70%, 34.67%, and 39.47% compared to the PP matrix for the PP/$CaCO_3$/Al-C LDH/0.5 GNPs, PP/$CaCO_3$/Al-C LDH/1.0 GNPs, PP/$CaCO_3$/Al-C LDH/1.5 GNPs, and PP/$CaCO_3$/Al-C LDH/2.0 GNPs hybrid composites, respectively. The compatibility between the polar and nonpolar components of the polymer blend plays a crucial role in enhancing the compressive strength of the composite polymers (Figures 12 and 13). This improvement is attributed to the nucleating effects of GNPs, the dispersion-strengthening effect of Al-C LDH in the PP matrix, and effective load transmission. Furthermore, it was noted that the addition of Al-C LDH improved the compressive mechanical properties compared to the PP/$CaCO_3$/x wt% GNPs hybrid composite (without Al-C LDH) discussed elsewhere [51]. For instance, the maximum ultimate compressive strength achieved in the PP/$CaCO_3$/1.5 GNPs hybrid composite sample (without Al-C LDH) was 54.77 MPa [51], whereas the PP/$CaCO_3$/Al-C LDH/2.0 GNPs hybrid composite sample exhibited 65.78 MPa, which is 20.10% higher than the sample without Al-C LDH in the same composition, due to the effective bonding and dispersion-strengthening effects of the introduced Al-C LDH.

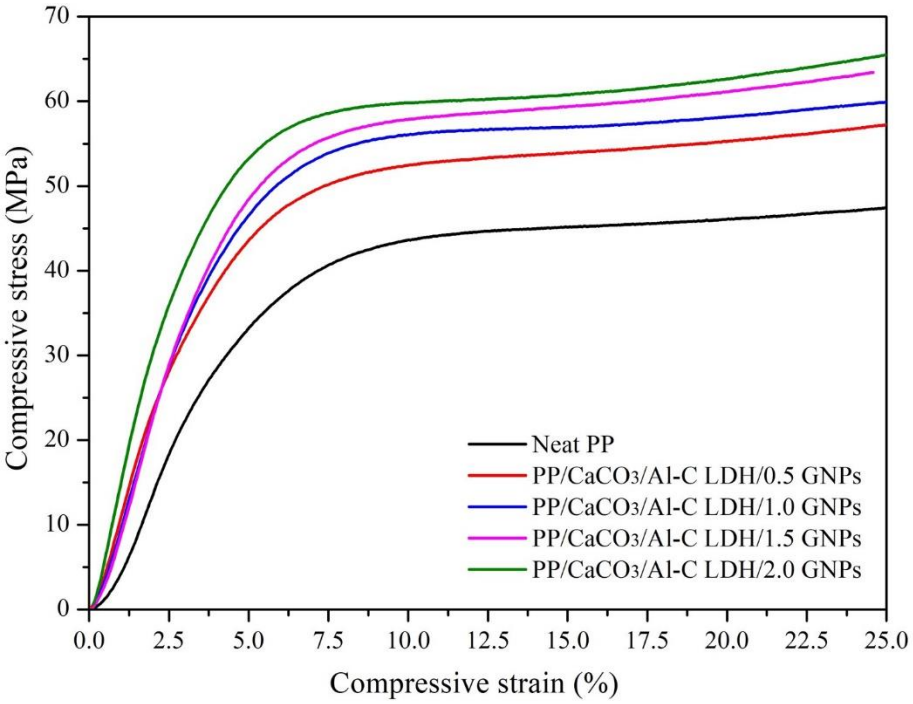

Figure 12. Compressive stress-strain curves of pure PP, PP/$CaCO_3$/Al-C LDH/0.5 GNPs, PP/$CaCO_3$/Al-C LDH/1.0 GNPs, PP/$CaCO_3$/Al-C LDH/1.5 GNPs, and PP/$CaCO_3$/Al-C LDH/2.0 GNPs hybrid composite polymers obtained from uniaxial compression test.

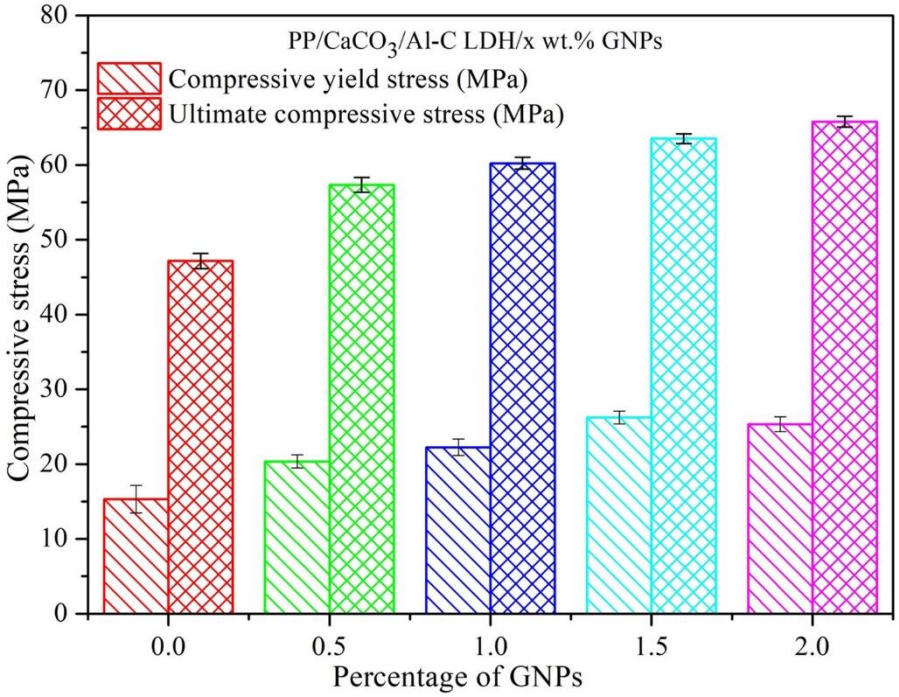

Figure 13. Compressive properties of developed pure PP matrix, PP/$CaCO_3$/Al-C LDH/0.5 GNPs, PP/$CaCO_3$/Al-C LDH/1.0 GNPs, PP/$CaCO_3$/Al-C LDH/1.5 GNPs, and PP/$CaCO_3$/Al-C LDH/2.0 GNPs hybrid composites.

Table 5. Mechanical properties of developed pure PP, PP/$CaCO_3$/Al-C LDH/0.5 GNPs, PP/$CaCO_3$/Al-C LDH/1.0 GNPs, PP/$CaCO_3$/Al-C LDH/1.5 GNPs, and PP/$CaCO_3$/Al-C LDH/2.0 GNPs hybrid composite polymers obtained from uniaxial compression test.

Sample ID	Compression moduli (MPa)	Compressive yield stress (MPa)	Compressive strain at yield point	Ultimate compressive stress (MPa)	Compressive strain at ultimate point
Neat PP	1620.358 ± 45.47	15.324 ± 1.85	0.0217 ± 0.005	47.169 ± 1.02	0.2504 ± 0.002
PP/$CaCO_3$/Al-C LDH/0.5 GNPs	2546.447 ± 39.87	20.365 ± 0.88	0.01789 ± 0.006	57.356 ± 0.98	0.2503 ± 0.003
PP/$CaCO_3$/Al-C LDH/1.0 GNPs	2692.254 ± 25.12	22.245 ± 1.10	0.02127 ± 0.004	60.236 ± 0.77	0.2504 ± 0.005
PP/$CaCO_3$/Al-C LDH/1.5 GNPs	3699.356 ± 24.451	26.236 ± 0.86	0.02687 ± 0.007	63.523 ± 0.65	0.2508 ± 0.003
PP/$CaCO_3$/Al-C LDH/2.0 GNPs	2985.341 ± 33.77	25.325 ± 0.98	0.02456 ± 0.003	65.789 ± 0.72	0.2504 ± 0.002

3.6.3. Flexural behavior

A three-point bending test was conducted to examine the flexural behavior in terms of flexural stress and flexural strain of the developed PP/$CaCO_3$/Al-C LDH/x wt% GNPs hybrid composites. Figure 14 shows the flexural stress-strain curves, and the corresponding flexural properties are listed in Table 6. The analysis of Figures 14, 15, and Table 6 clearly indicates that the flexural strength of the PP/$CaCO_3$/Al-C LDH/x wt% GNPs hybrid composite polymers significantly increases with the incorporation of GNPs and Al-C LDH. This improvement is attributed to the effective interaction between the GNPs, $CaCO_3$, Al-C LDH, and the PP matrix, the uniform dispersion of GNPs, $CaCO_3$, and Al-C LDH within the PP matrix, and the barrier effect provided by the GNPs, among other factors discussed earlier. It was observed that the incorporation of 2 wt% Al-C LDH in PP/$CaCO_3$/x wt% GNPs hybrid composites enhanced the flexural properties [51]. For example, the highest flexural strength obtained in the PP/$CaCO_3$/1.5 GNPs hybrid composite polymer (without Al-C LDH) was 57.12 MPa. However, with the incorporation of 2 wt% Al-C LDH, the PP/$CaCO_3$/Al-C LDH/1.5 GNPs hybrid composite sample exhibited the highest flexural strength of 64.54 MPa, which is approximately 13% greater compared to the PP/$CaCO_3$/1.5 GNPs hybrid composite polymer (without Al-C LDH). These results further confirm the benefits of introducing Al-C LDH for enhancing the strength of the PP matrix.

Table 6. Flexural properties of developed pure PP, PP/$CaCO_3$/Al-C LDH/0.5 GNPs, PP/$CaCO_3$/Al-C LDH/1.0 GNPs, PP/$CaCO_3$/Al-C LDH/1.5 GNPs, and PP/$CaCO_3$/Al-C LDH/2.0 GNPs hybrid composite polymers obtained from 3P bending test.

Sample	Flexural stress (MPa)	Flexural modulus (MPa)	Modulus of toughness (J/mm^3)
Pure PP	46.572 ± 3.28	371.323 ± 1.25	30.979 ± 0.85
PP/$CaCO_3$/Al-C LDH/0.5 GNPs	55.368 ± 4.94	422.547 ± 0.98	54.471 ± 0.65
PP/$CaCO_3$/Al-C LDH/1.0 GNPs	61.254 ± 3.97	431.554 ± 1.10	58.778 ± 0.75
PP/$CaCO_3$/Al-C LDH/1.5 GNPs	64.539 ± 2.47	436.251 ± 0.85	61.547 ± 0.97
PP/$CaCO_3$/Al-C LDH/2.0 GNPs	62.325 ± 2.45	433.522 ± 1.13	60.875 ± 1.05

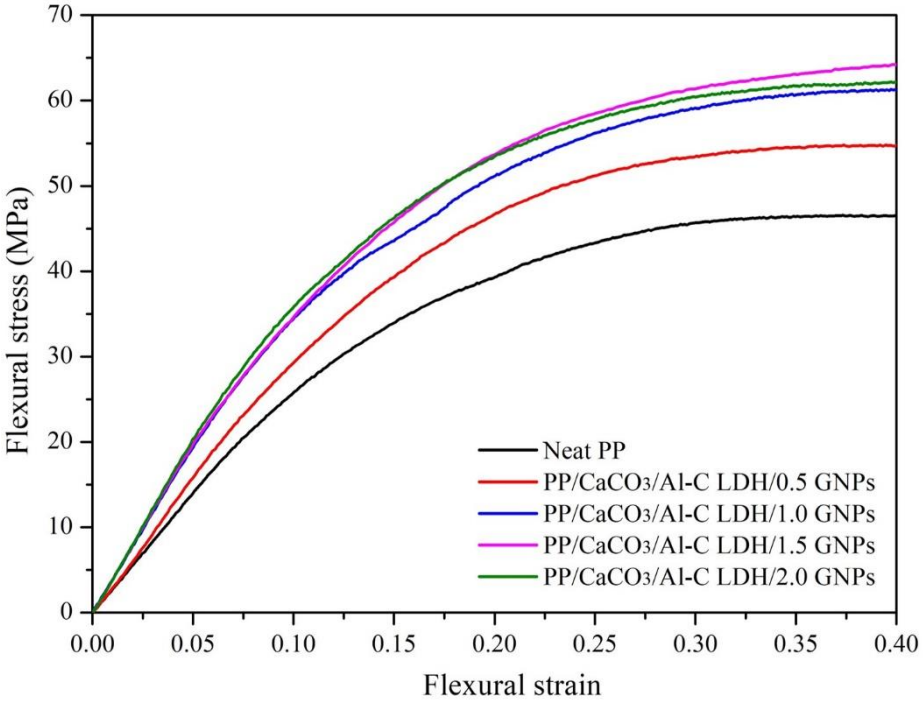

Figure 14. Flexural stress-strain curves of pure PP, PP/$CaCO_3$/Al-C LDH/0.5 GNPs, PP/$CaCO_3$/Al-C LDH/1.0 GNPs, PP/$CaCO_3$/Al-C LDH/1.5 GNPs, and PP/$CaCO_3$/Al-C LDH/2.0 GNPs hybrid composite polymers obtained from 3P bending test.

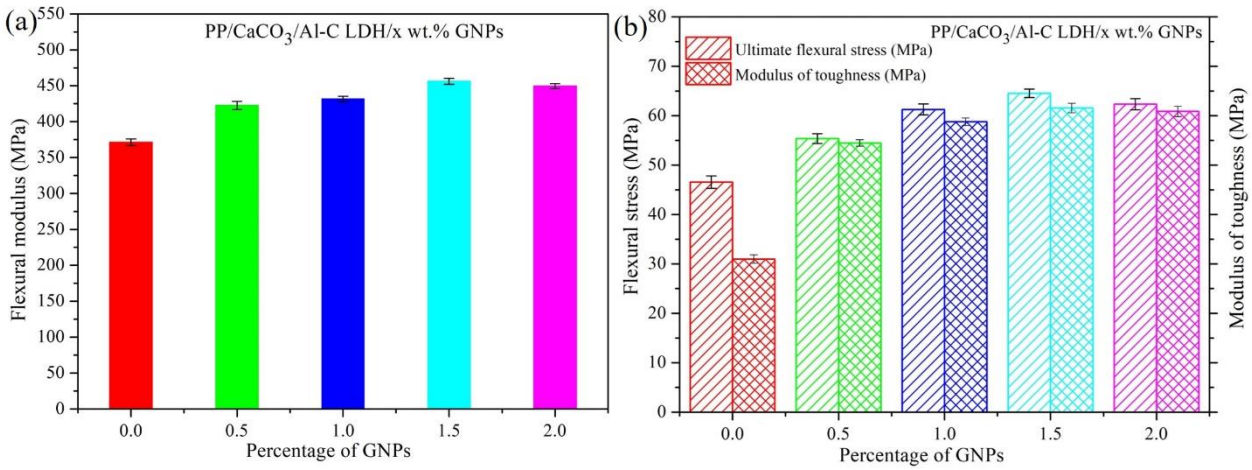

Figure 15. Flexural properties: (a) flexural modulus and (b) flexural stress and modulus of toughness of developed pure PP matrix, PP/$CaCO_3$/Al-C LDH/0.5 GNPs, PP/$CaCO_3$/Al-C LDH/1.0 GNPs, PP/$CaCO_3$/Al-C LDH/1.5 GNPs, and PP/$CaCO_3$/Al-C LDH/2.0 GNPs hybrid composites.

3.6.4. Low-velocity impact test

A low-velocity impact test was conducted on the developed PP/$CaCO_3$/Al-C LDH/x wt% GNPs hybrid composites to examine their impact behavior. The low-velocity impact test was performed using a CEAST 9350 Instron machine, which consists of an impactor insert, an anti-rebound system, a lubricating system, a photocell for data recording, and a high-energy configuration positioning system. A hemispheric impact insert with a diameter of 20 mm and a length of 40 mm was used. The photocell was aligned with the tip of the insert and the specimen's surface for accurate data measurement. The specimen was securely held in place by an automatic clamping ring with a clamping pressure of 5.5 bars. The details of the parameters used in the low-velocity impact testing of the hybrid composite samples are explained elsewhere [51]. Impact velocity refers to the speed at which the impactor contacts the specimen surface. A load cell embedded within the impactor head recorded the vertical force over time to determine impact characteristics. Results shown in Figure 16 indicate that the addition of GNPs and Al-C LDH significantly increased the peak impact force and energy in the hybrid composites of PP/$CaCO_3$/Al-C LDH/x wt% GNPs. Additionally, the residual velocity decreased notably as the GNP and Al-C LDH content in PP increased. The improved impact properties are attributed to the nucleating effects of the GNPs and Al-C LDH in PP, strong interactions between the GNPs, Al-C LDH, and PP, and effective dispersion of GNPs and Al-C LDH, as discussed in a previous section. It was observed that the incorporation of 2 wt% Al-C LDH enhanced the impact performance of the developed PP/$CaCO_3$/Al-C LDH/x wt% GNPs hybrid composites compared to the PP/$CaCO_3$/x wt% GNPs hybrid composite polymer samples (without Al-C LDH). For instance, the highest impact force observed in the PP/$CaCO_3$/1.5 wt% GNPs hybrid polymer (without Al-C LDH) was 8250 N, whereas the highest impact force observed in the PP/$CaCO_3$/Al-C LDH/1.5 wt% GNPs hybrid polymer (with Al-C LDH) was 8610 N, which is approximately 4.4% higher compared to the sample without Al-C LDH of the same composition. These results further confirm the improvement of properties in the hybrid composite polymers with the incorporation of Al-C LDH.

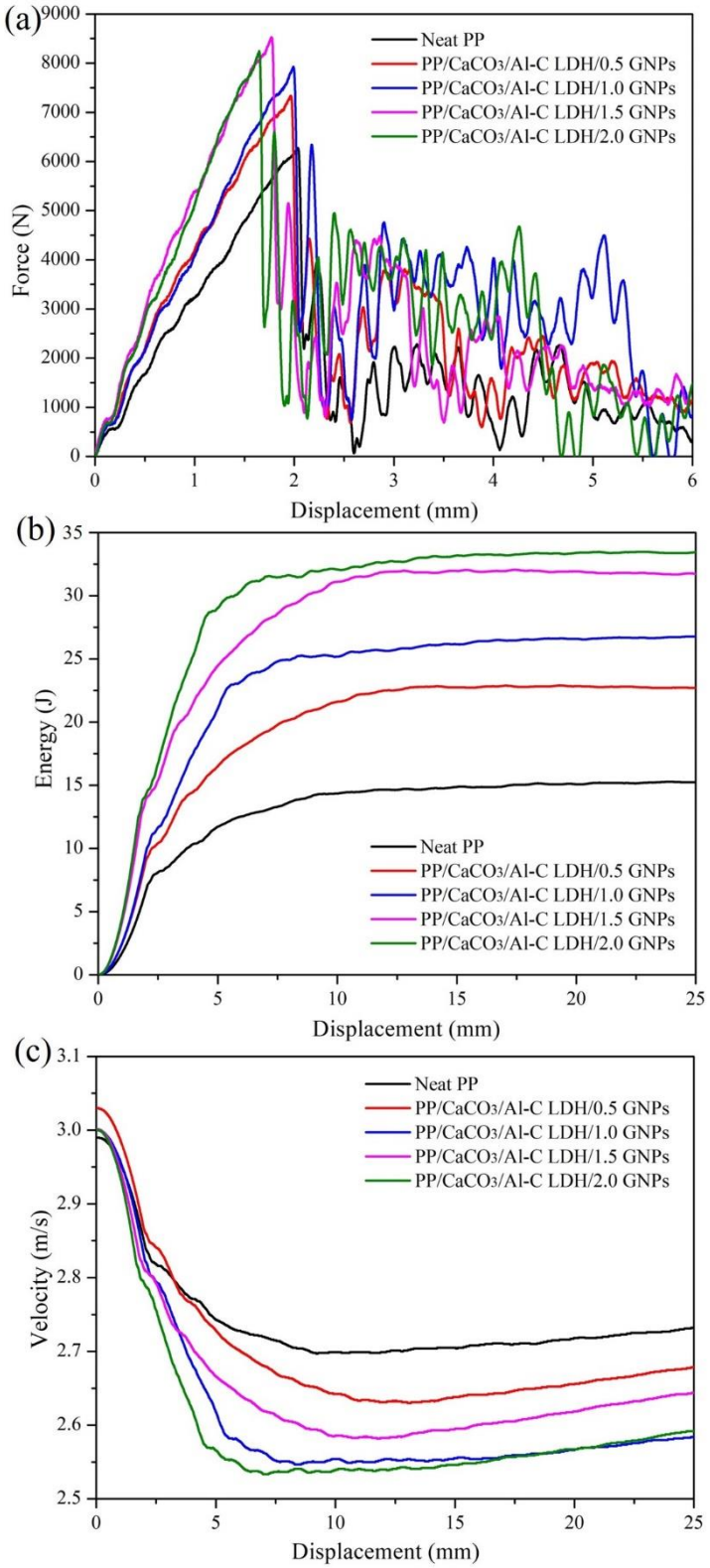

Figure 16. Low-velocity behavior of the pure PP, PP/$CaCO_3$/Al-C LDH/0.5 GNPs, PP/$CaCO_3$/Al-C LDH/1.0 GNPs, PP/$CaCO_3$/Al-C LDH/1.5 GNPs, and PP/$CaCO_3$/Al-C LDH/2.0 GNPs hybrid composite polymers: (a) force Vs displacement profile; (b) energy Vs displacement profile; and (c) velocity Vs displacement profile.

3.7. Nanoindentation test

Figure 17a displays the load-displacement curves for the developed pure PP, PP/$CaCO_3$/Al-C LDH/1.0 GNPs, and PP/$CaCO_3$/Al-C LDH/2.0 GNPs hybrid nanocomposites. The curve shows that incorporating 2 wt% GNPs, along with the uniform dispersion of $CaCO_3$ and Al-C LDH, enhances the elastic recovery of the PP/$CaCO_3$/Al-C LDH/2.0 GNPs hybrid composite samples. In contrast, the blended sample with 0 wt% GNPs (i.e., neat PP) in the matrix exhibits reduced elastic recovery due to the lack of dispersed reinforcement. Additionally, the particle dispersion strengthening mechanism in the hybrid composite is primarily responsible for the curve's shift from right to left, indicating a decrease in displacement. Figure 17b,c illustrate the variation in hardness and elastic modulus of the pure PP, PP/$CaCO_3$/Al-C LDH/1.0 GNPs, and PP/$CaCO_3$/Al-C LDH/2.0 GNPs hybrid composite polymers. These properties were measured concerning the wt% of GNPs during nanoindentation at a maximum load of 10 mN. The results indicate that both hardness and elastic modulus increase as the GNP content rises. Consequently, the PP/$CaCO_3$/Al-C LDH/2.0 GNPs hybrid composite demonstrates greater hardness and elastic modulus compared to the pure PP matrix. This improvement is attributed to the 2 wt% increase in GNPs combined with the presence of $CaCO_3$ and Al-C LDH particles. The modulus of elasticity obtained from tensile tests (macro-scale) and nanoindentation (micro-scale) revealed notable variations. This difference was attributed to the localized nature of nanoindentation, where the indenter interacts with most of the reinforced regions or areas where GNPs were more homogeneously dispersed, resulting in higher hardness and modulus values. Conversely, tensile testing provides an averaged response of the entire composite, which includes regions with agglomerated GNPs and inhomogeneous reinforcement distribution, leading to lower bulk modulus values.

The mechanical properties obtained from tensile tests of the PP matrix reinforced with different weight percentages of fillers—namely GNPs, MWCNTs, talc, MgAl LDH, MgCoAl LDHs, MgNiAl LDHs, MgCuAl LDHs, MgZnAl LDHs, ammonium polyphosphate (APP) LDHs, $CaCO_3$, and Al-C LDHs—are compared and presented in Table 7. It is clear that the incorporation of various fillers into the PP matrix has improved its mechanical properties. Among the incorporated fillers, GNPs significantly enhance the mechanical properties of the PP matrix. Specifically, the PP/$CaCO_3$/Al-C LDH/1.5 GNPs hybrid composite (current work) achieved higher mechanical properties, with an ultimate tensile strength of 44.85 MPa, compared to the results from previous studies [5,18,24,27,30,37, 49–51,57,61].

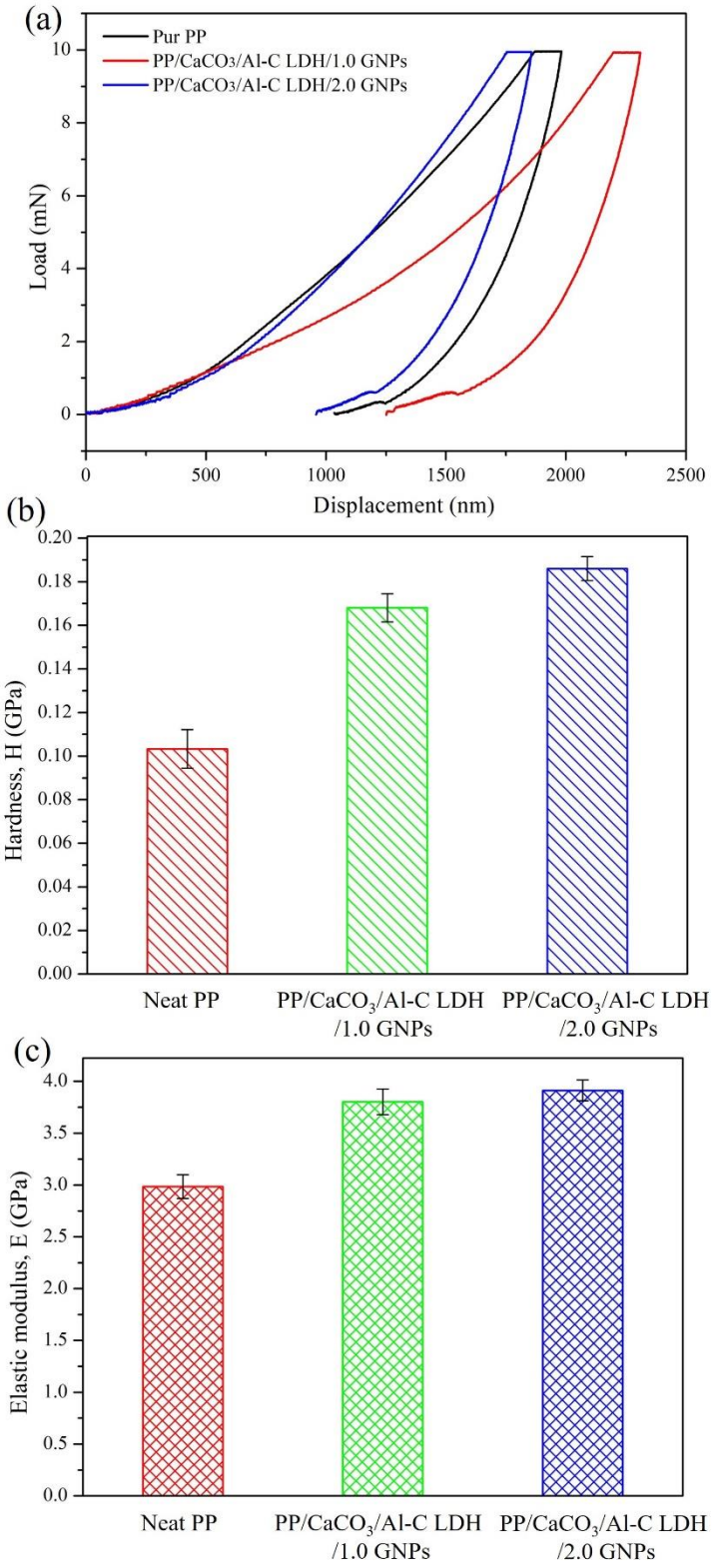

Figure 17. Nanoindentation test of pure PP, PP/$CaCO_3$/Al-C LDH/1.0 GNPs, and PP/$CaCO_3$/Al-C LDH/2.0 GNPs hybrid composite polymers: (a) load-displacement curves; (b) hardness; and (c) elastic modulus.

Table 7. Comparison of mechanical properties of PP matrix reinforced with different fillers/LDH between several research works and the present one.

No.	Name of matrix materials and reinforcements	Modulus of elasticity (MPa)	Ultimate tensile stress (MPa)	Ref.
1	PP embedded with 3.5 wt% GNPS	1669.9	42.6	[49]
2	PP reinforced with 0.5 wt% MWCNTs	261.41	18.88	[61]
3	HDPE reinforced with 1 wt% GNPs	-	23	[24]
4	PP reinforced with 10 wt% talc	489	25	[5]
5	PP embedded with 15 wt% calcium carbonates	2015	28	[18]
6	PP embedded with 0.8 wt% GNPs	-	32	[50]
7	PP reinforced with w wt% MgAl LDHs	1710	34.3	[30]
	PP reinforced with 5 wt% MgCoAl LDHs	1745	34.6	
	PP reinforced with 5 wt% MgNiAl LDHs	1713	34.2	
	PP reinforced with 5 wt% MgCuAl LDHs	1783	35.0	
	PP reinforced with 5 wt% MgZnAl LDHs	1767	34.8	
8	HDPE reinforced with 10 wt% GNPs	1490	33.4	[27]
	HDPE reinforced with 0.25 wt% GNPs	1290	30.5	
9	PP reinforced with 10 wt% ammonium polyphosphate (APP) LDHs	-	18	[37]
	PP reinforced with 10 wt % APP LDHs and 2 wt% ZB	-	16	
10	PP reinforced with 5 wt% GNPs	1900	32.8	[62]
11	PP reinforced with 2 wt% $CaCO_3$, 1.5 wt% GNPs	2923	40.546	[51]
12	PP reinforced with 2 wt% $CaCO_3$, 2 wt% Al-C LDH, and 1.5 wt% GNPs	3891.19	44.85	Current work

3.8. Fracture surface topography analyses

In this study, SEM fracture surface analysis was conducted on the fractured areas from tensile and impact tests, with the results depicted in Figures 18 and 19, respectively. The SEM images revealed that the pure PP matrix exhibited a ductile morphology with regular wave-like patterns, indicative of expansion and effective cross-linking (Figure 18a–c). No cracks, voids, or inclusions were observed in the pure PP matrix. Conversely, the PP/$CaCO_3$/Al-C LDH/1.0 GNPs and PP/$CaCO_3$/Al-C LDH/2.0 GNPs hybrid composite samples displayed brittle or mixed ductile-brittle fracture surfaces (Figure 18d–i). The PP/$CaCO_3$/Al-C LDH/1.0 GNPs hybrid composite showed rough surfaces with uniform GNP pull-outs, suggesting effective load transfer between the GNPs and the PP matrix (Figure 18d–f). In contrast, the PP/$CaCO_3$/Al-C LDH/2.0 GNPs hybrid composite exhibited very rough surfaces with numerous voids, cracks, cleavage patterns, and non-uniform GNP pull-outs, attributed to GNP agglomeration and defects (Figure 18g–i). Consequently, the PP/$CaCO_3$/Al-C LDH/2.0 GNPs hybrid composite displayed lower mechanical properties (Tables 4–6). It was concluded that increasing the GNP content up to 1.5 wt% improved the microstructural features and mechanical properties due to better dispersion, load transfer, and uniform dislocations. However,

exceeding 1.5 wt% GNPs resulted in more defects and uneven dispersion, leading to brittle fractures and reduced mechanical properties. Similarly, after impact tests, the pure PP matrix exhibited a homogeneous ductile fracture surface, attributed to proper cross-linking and the absence of defects (Figure 19a–c). The PP/$CaCO_3$/Al-C LDH/1.0 GNPs hybrid composite displayed a slightly rough surface with a brittle flat area (Figure 19d–f). The PP/$CaCO_3$/Al-C LDH/2.0 GNPs hybrid composite showed a severely rough and completely brittle fracture surface with extensive damage, indicating more defects and weaker bonding, which led to deteriorated mechanical properties (Figure 19g–i).

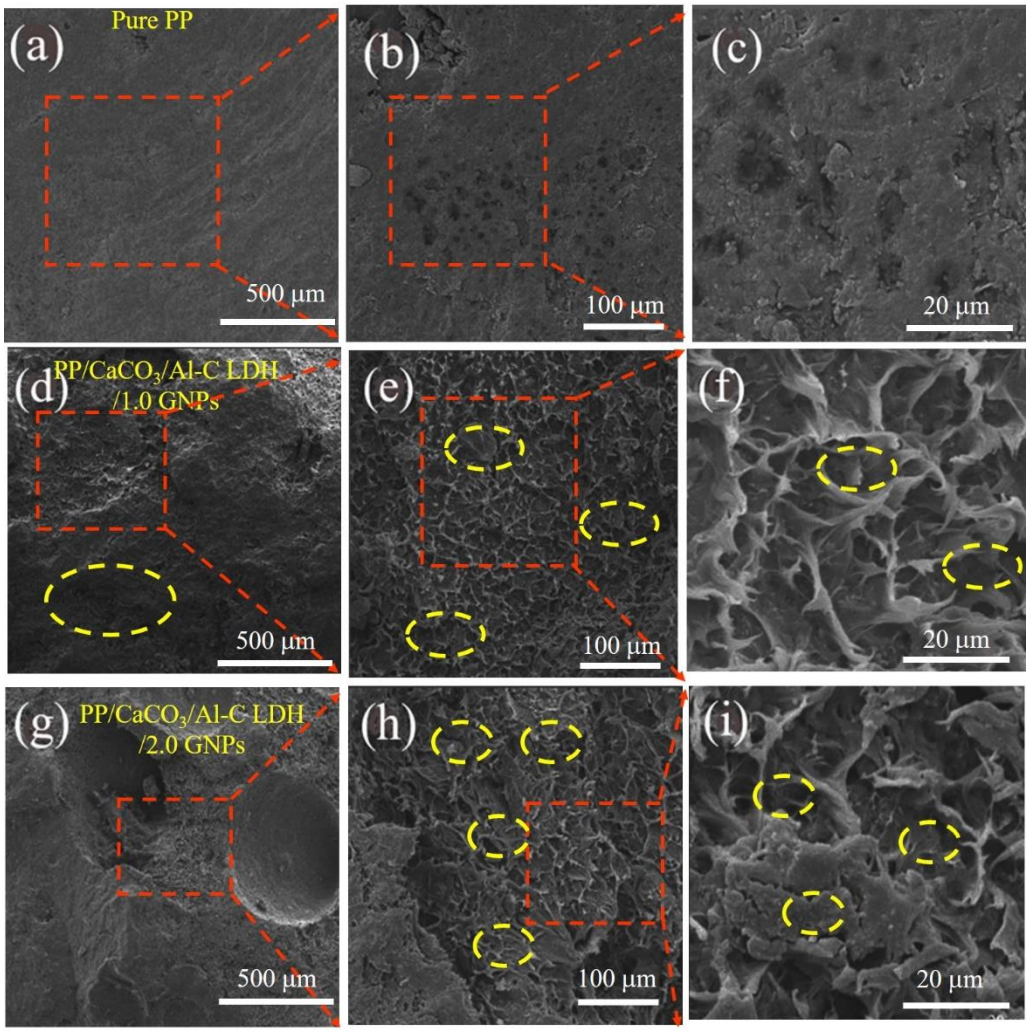

Figure 18. SEM microstructure of fractured area after tensile test of (a–c) pure PP; (d–f) PP/$CaCO_3$/Al-C LDH/1.0 GNPs; and (g–i) PP/$CaCO_3$/Al-C LDH/2.0 GNPs hybrid composites. Yellow dashed circles represent the presence of GNPs/Al-C LDH/$CaCO_3$ fillers over the PP matrix.

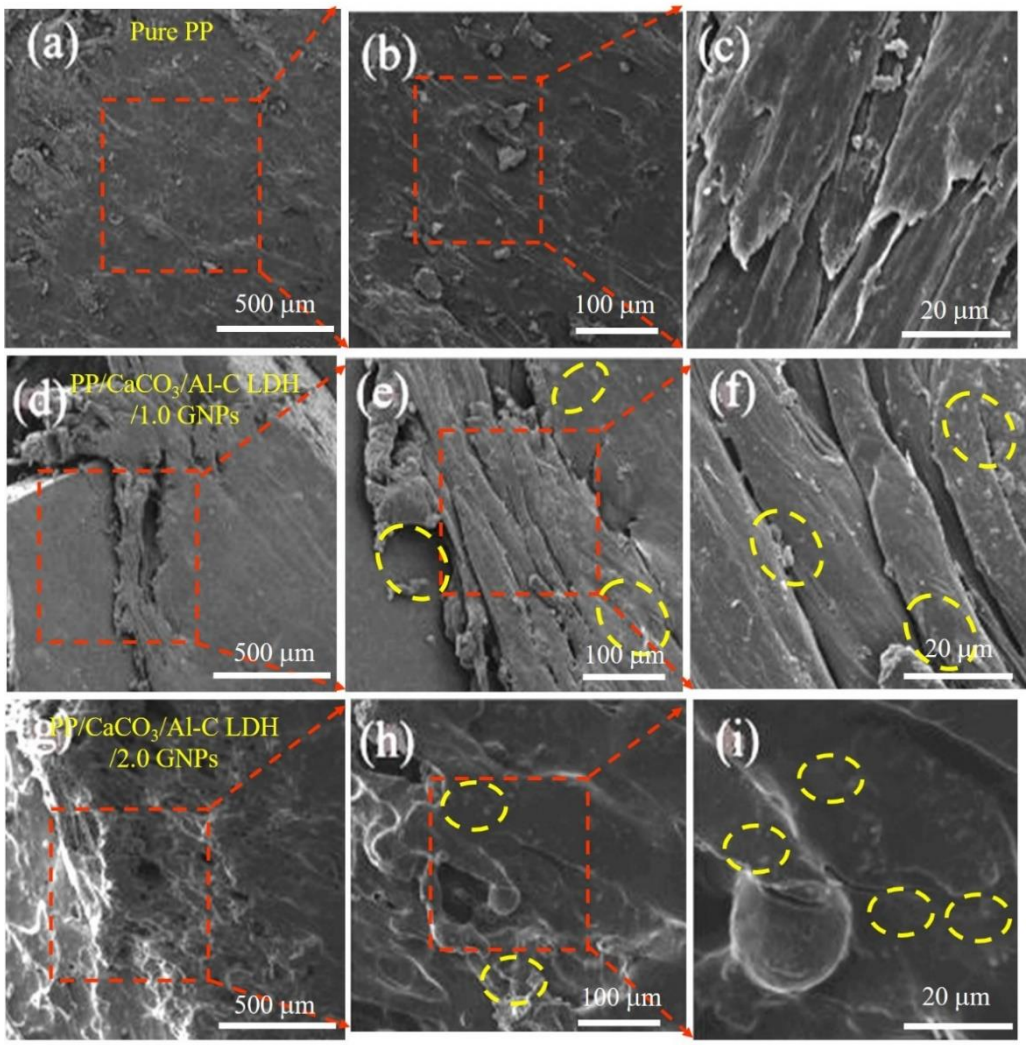

Figure 19. SEM microstructure of fractured area after impact test of (a–c) pure PP; (d–f) PP/$CaCO_3$/Al-C LDH/1.0 GNPs; and (g–i) PP/$CaCO_3$/Al-C LDH/2.0 GNPs hybrid composites. Yellow dashed circles represent the location of GNPs/Al-C LDH/$CaCO_3$ fillers over the PP matrix.

4. Conclusions

- Four polymer composites reinforced with GNPs and Al-C LDH (namely PP/$CaCO_3$/Al-C LDH/0.5 GNPs, PP/$CaCO_3$/Al-C LDH/1.0 GNPs, PP/$CaCO_3$/Al-C LDH/1.5 GNPs, and PP/$CaCO_3$/Al-C LDH/2.0 GNPs), along with pure PP, were successfully synthesized using melt compounding (twin extrusion) followed by injection molding.
- Macroscopic and microscopic examinations confirmed the purity and morphology of the as-received polymers.
- The synthesized polymer composites were characterized using FTIR, XPS, XRD, and TGA. FTIR and XPS results indicated strong bonding between the polymer, GNPs, and Al-C LDH. FTIR analysis showed symmetric vibrations in the ranges of 2963–3015 and 2815–2962 cm^{-1}, confirming

the presence of the infused polymer and the strong bonding of the incorporated GNPs and Al-C LDH within the PP matrix.

- XRD results revealed a shift in the peak positions of the α-form PP matrix with an increase in GNP loading, which was attributed to the significant interfacial tension between the incorporated GNPs and the PP matrix. The PP/$CaCO_3$/Al-C LDH/2.0 GNPs hybrid composite showed higher thermal stability compared to neat PP in thermogravimetric analysis, indicating good compatibility of Al-C LDH with GNPs in the PP matrix.
- Mechanical properties were evaluated through tensile tests, compression tests, and three-point bending tests, demonstrating enhanced mechanical properties due to the integration of GNPs and Al-C LDH.
- Low-velocity impact tests also showed improved peak force, increased energy absorption, and enhanced residual velocity with the addition of GNPs and Al-C LDH, attributed to the effective dispersion and strong bonding between these components and the PP matrix.
- HRSEM fracture surface analysis revealed ductile and defect-free surfaces in the pure PP matrix, while a combination of ductile and brittle fractures with rough surfaces was observed in the composites with GNPs and Al-C LDH. The incorporation of up to 1.0 wt% GNPs improved microstructural features and load transfer efficiency. However, the PP/$CaCO_3$/Al-C LDH/2.0 GNPs sample exhibited severe rough surfaces with more defects (cracks, cleavages, and voids), leading to decreased mechanical properties.
- Among the developed samples, the PP/$CaCO_3$/Al-C LDH/1.0 GNPs composite exhibited the best thermal and mechanical properties, making it suitable for structural and other applications.

Use of AI tools declaration

The authors declare they have not used Artificial Intelligence (AI) tools in the creation of this article.

Author contributions

Conceptualization: D.B., R.K., S.S., A.E.; validation: D.B., R.K., S.S., M.S.; formal analysis: D.B., A.A., R.K.; investigation: R.K., S.S., M.S., A.A.; resources: R.K., S.S., A.A.; data curation: R.K., S.S., M.S., A.A.; writing—original draft preparation: R.K., S.S., M.S., A.A.; writing—review and editing: S.S., M.S., A.A.; supervision: R.K., S.S., M.S. All authors have read and agreed to the published version of the manuscript.

Conflicts of interest

The authors declare no conflict of interest.

Data availability statement

The experimental datasets obtained from this research work and then the analyzed results during the current study are available from the corresponding author upon reasonable request.

References

1. Cheng Q, Jiang CK, Zhang JW, et al. (2016) Effect of thermal aging on the scratch behavior of poly (methyl methacrylate). *Tribol Int* 101: 110–114. https://doi.org/10.1016/j.triboint.2016.04.013
2. Gao WM, Wang L, Coffey JK, et al. (2018) Understanding the scratch behaviour of polymeric materials with surface texture. *Mater Des* 146: 38–48. https://doi.org/10.1016/j.matdes.2018.02.074
3. Friedrich K, Sue HJ, Liu P, et al. (2011) Scratch resistance of high performance polymers. *Tribol Int* 44: 1032–1046. https://doi.org/10.1016/j.triboint.2011.04.008
4. Mae H (2009) Characterization of material ductility of PP/EPR/talc blend under wide range of stress triaxiality at intermediate and high strain rates. *J Appl Polym Sci* 111: 854–868. https://doi.org/10.1002/app.29069
5. Kant S, Urmila, Kumar J, et al. (2013) Study of talc filled polypropylene—A concept for improving mechanical properties of polypropylene. *Int J Res Eng Technol* 02: 411–415. https://doi.org/10.15623/ijret.2013.0204001
6. Xiang C, Sue H, Chu J, et al. (2001) Roles of additives in scratch resistance of high crystallinity polypropylene copolymers. *Polym Eng Sci* 41: 23–31. https://doi.org/10.1002/pen.10705
7. Jerabek M, Tscharnuter D, Major Z, et al. (2010) Relaxation behavior of neat and particulate filled polypropylene in uniaxial and multiaxial compression. *Mech Time-Depend Mater* 14: 47–68. https://doi.org/10.1007/s11043-009-9092-y
8. Hartl AM, Jerabek M, Lang RW (2015) Anisotropy and compression/tension asymmetry of PP containing soft and hard particles and short glass fibers. *Express Polym Lett* 9: 658–670. https://doi.org/10.3144/expresspolymlett.2015.61
9. Panamoottil SM, Das R, Jayaraman K (2016) Anisotropic continuum damage model for prediction of failure in flax/polypropylene fabric composites. *Polym Compos* 37: 2588–2597. https://doi.org/10.1002/pc.23453
10. Misra RDK, Hadal R, Duncan SJ (2004) Surface damage behavior during scratch deformation of mineral reinforced polymer composites. *Acta Mater* 52: 4363–4376. https://doi.org/10.1016/j.actamat.2004.06.003
11. Dasari A, Yu ZZ, Mai YW (2009) Fundamental aspects and recent progress on wear/scratch damage in polymer nanocomposites. *Mater Sci Eng R Reports* 63: 31–80. https://doi.org/10.1016/j.mser.2008.10.001
12. Chu J, Rumao L, Coleman B (1998) Scratch and mar resistance of filled polypropylene materials. *Polym Eng Sci* 38: 1906–1914. https://doi.org/10.1002/pen.10361
13. Chu J, Xiang C, Sue H, et al. (2000) Scratch resistance of mineral-filled polypropylene materials. *Polym Eng Sci* 40: 944–955. https://doi.org/10.1002/pen.11222
14. Moghbelli E, Browning RL, Boo WJ, et al. (2008) Effects of molecular weight and thermal history on scratch behavior of polypropylene thin sheets. *Tribol Int* 41: 425–433. https://doi.org/10.1016/j.triboint.2007.09.008
15. Maspoch ML, Gamez-Perez J, Gimenez E, et al. (2004) Influence of processing on ethylene-propylene block copolymers: Structure and mechanical behavior. *J Appl Polym Sci* 93: 2866–2878. https://doi.org/10.1002/app.20834

16. Da Silva ALN, Rocha MCG, Lopes L, et al. (2001) The effect of addition of different elastomers upon the crystalline nature of PP. *J Appl Polym Sci* 81: 3530–3537. https://doi.org/10.1002/app.1809
17. Karger-Kocsis J (2012) *Polypropylene: An A–Z Reference*, New York: Springer Dordrecht. https://doi.org/10.1007/978-94-011-4421-6
18. Zokaei S, Bagheri R (2007) Study of scratch resistance in homo-and co-polypropylene filled with nanometric calcium carbonate. *Mater Sci Eng A* 445: 526–536. https://doi.org/10.1016/j.msea.2006.09.080
19. Dasari A, Rohrmann J, Misra RDK (2002) Micro-and nanoscale evaluation of scratch damage in poly(propylene)s. *Macromol Mater Eng* 287: 889–903. https://doi.org/10.1002/mame.200290024
20. Dasari A, Rohrmann J, Misra RDK (2003) Atomic force microscopy assessment of mechanically induced scratch damage in polypropylenes and ethylene–propylene di-block copolymers. *Mater Sci Eng A* 354: 67–81. https://doi.org/10.1016/S0921-5093(02)00873-0
21. Wong M, Lim GT, Moyse A, et al. (2004) A new test methodology for evaluating scratch resistance of polymers. *Wear* 256: 1214–1227. https://doi.org/10.1016/j.wear.2003.10.027
22. Ravishankar B, Nayak SK, Kader MA (2019) Hybrid composites for automotive applications–A review. *J Reinf Plast Compos* 38: 835–845. https://doi.org/10.1177/0731684419849708
23. Kufel A, Para S, Kuciel S (2021) Basalt/glass fiber polypropylene hybrid composites: Mechanical properties at different temperatures and under cyclic loading and micromechanical modelling. *Materials (Basel)* 14: 5574. https://doi.org/10.3390/ma14195574
24. Seretis GV, Manolakos DE, Provatidis CG (2018) On the graphene nanoplatelets reinforcement of extruded high density polyethylene. *Compos Part B Eng* 145: 81–89. https://doi.org/10.1016/j.compositesb.2018.03.020
25. Cataldi P, Athanassiou A, Bayer IS (2018) Graphene nanoplatelets-based advanced materials and recent progress in sustainable applications. *Appl Sci* 8: 1438. https://doi.org/10.3390/app8091438
26. Chung DDL (2016) A review of exfoliated graphite. *J Mater Sci* 51: 554–568. https://doi.org/10.1007/s10853-015-9284-6
27. Lin S, Anwer MAS, Zhou Y, et al. (2018) Evaluation of the thermal, mechanical and dynamic mechanical characteristics of modified graphite nanoplatelets and graphene oxide high-density polyethylene composites. *Compos Part B Eng* 132: 61–68. https://doi.org/10.1016/j.compositesb.2017.08.010
28. Feng J, Safaei B, Qin Z, et al. (2023) Nature-inspired energy dissipation sandwich composites reinforced with high-friction graphene. *Compos Sci Technol* 233: 109925. https://doi.org/10.1016/j.compscitech.2023.109925
29. Wang P, Zhang X, Zhou B, et al. (2023) Recent advance of layered double hydroxides materials: Structure, properties, synthesis, modification and applications of wastewater treatment. *J Environ Chem Eng* 11: 111191. https://doi.org/10.1016/j.jece.2023.111191
30. Naseem S, Wießner S, Kühnert I, et al. (2023) Polypropylene (PP) nanocomposites with transition metal (MgCoAl, MgNiAl, MgCuAl, MgZnAl) layered double hydroxides (t-LDHs): Flammability, thermal and mechanical analysis. *Adv Ind Eng Polym Res* 6: 203–213. https://doi.org/10.1016/j.aiepr.2023.01.007
31. Oosthuizen H, Jones L, Naseem S, et al. (2023) Tailoring materials for their need: Sustainable layered double hydroxide polymer composites. *J Polym Sci* 61: 1749–1777. https://doi.org/10.1002/pol.20230025

32. Mishra G, Dash B, Pandey S (2018) Layered double hydroxides: A brief review from fundamentals to application as evolving biomaterials. *Appl Clay Sci* 153: 172–186. https://doi.org/10.1016/j.clay.2017.12.021
33. Alagha O, Manzar MS, Zubair M, et al. (2020) Comparative adsorptive removal of phosphate and nitrate from wastewater using biochar-MgAl LDH nanocomposites: Coexisting anions effect and mechanistic studies. *Nanomaterials* 10: 336. https://doi.org/10.3390/nano10020336
34. Lin YJ, Li DQ, Evans DG, et al. (2005) Modulating effect of Mg–Al–CO_3 layered double hydroxides on the thermal stability of PVC resin. *Polym Degrad Stab* 88: 286–293. https://doi.org/10.1016/j.polymdegradstab.2004.11.007
35. Lonkar SP, Leuteritz A, Heinrich G (2013) Antioxidant intercalated layered double hydroxides: A new multifunctional nanofiller for polymers. *RSC Adv* 3: 1495–1501. https://doi.org/10.1039/C2RA21956E
36. Fan G, Li F, Evans DG, et al. (2014) Catalytic applications of layered double hydroxides: Recent advances and perspectives. *Chem Soc Rev* 43: 7040–7066. https://doi.org/10.1039/C4CS00160E
37. Gao Y, Wang Q, Lin W (2018) Ammonium polyphosphate intercalated layered double hydroxide and zinc borate as highly efficient flame retardant nanofillers for polypropylene. *Polymers (Basel)* 10: 1114. https://doi.org/10.3390/polym10101114
38. Naseem S, Lonkar SP, Leuteritz A, et al. (2018) Different transition metal combinations of LDH systems and their organic modifications as UV protecting materials for polypropylene (PP). *RSC Adv* 8: 29789–29796. https://doi.org/10.1039/C8RA05447A
39. Naseem S, Gevers BR, Labuschagné FJWJ, et al. (2020) Preparation of photoactive transition-metal layered double hydroxides (LDH) to replace dye-sensitized materials in solar cells. *Materials (Basel)* 13: 4384. https://doi.org/10.3390/ma13194384
40. Yang G, Takei T, Yanagida S, et al. (2019) Enhanced supercapacitor performance based on CoAl layered double hydroxide-polyaniline hybrid electrodes manufactured using hydrothermal-electrodeposition technology. *Molecules* 24: 976. https://doi.org/10.3390/molecules24050976
41. Zhang C, Liang X, Lu Y, et al. (2020) Performance of CuAl-LDH/Gr nanocomposite-based electrochemical sensor with regard to trace glyphosate detection in water. *Sensors* 20: 4146. https://doi.org/10.3390/s20154146
42. Camino G, Maffezzoli A, Braglia M, et al. (2001) Effect of hydroxides and hydroxycarbonate structure on fire retardant effectiveness and mechanical properties in ethylene-vinyl acetate copolymer. *Polym Degrad Stab* 74: 457–464. https://doi.org/10.1016/S0141-3910(01)00167-7
43. Wang X, Zhang Q (2004) Effect of hydrotalcite on the thermal stability, mechanical properties, rheology and flame retardance of poly(vinyl chloride). *Polym Int* 53: 698–707. https://doi.org/10.1002/pi.1482
44. Jiang T, Liu C, Liu L, et al. (2016) Synergistic flame retardant properties of a layered double hydroxide in combination with zirconium phosphonate in polypropylene. *RSC Adv* 6: 91720–91727. https://doi.org/10.1039/C6RA15542A
45. Qiu L, Gao Y, Zhang C, et al. (2018) Synthesis of highly efficient flame retardant polypropylene nanocomposites with surfactant intercalated layered double hydroxides. *Dalt Trans* 47: 2965–2975. https://doi.org/10.1039/C7DT03477F
46. Ghabezi P, Farahani M, Fakhr M, et al. (2016) Investigation of mechanical behavior of Alfa and gamma nano-alumina/epoxy composite made by vartm. *Int J Adv Biotechnol Res* 7: 731–736. Available from: https://www.researchgate.net/publication/310298603.

47. Ghabezi P, Farahani M, Fakhr MH (2016) Experimental investigation of nano-alumina effect on the filling time in VARTM process. *J Fundam Appl Sci* 8: 925–940. https://www.ajol.info/index.php/jfas/article/view/142589
48. Wang H, Pei X, Shao R, et al. (2023) Resistance of graphene/epoxy resin—based composite materials to γ radiation damage and their mechanical properties. *Coatings* 13: 1536. https://doi.org/10.3390/coatings13091536
49. Zhao X, Huang D, Ewulonu CM, et al. (2021) Polypropylene/graphene nanoplatelets nanocomposites with high conductivity via solid-state shear mixing. *e-Polymers* 21: 520–532. https://doi.org/10.1515/epoly-2021-0039
50. Sheshmani S, Ashori A, Fashapoyeh MA (2013) Wood plastic composite using graphene nanoplatelets. *Int J Biol Macromol* 58: 1–6. https://doi.org/10.1016/j.ijbiomac.2013.03.047
51. Banu RD, Karunanithi R, Sivasankaran S, et al. (2024) Synthesis, characterization, thermal and mechanical behavior of polypropylene hybrid composites embedded with $CaCO_3$ and graphene nano-platelets (GNPs) for structural applications. *AIMS Mater Sci* 11: 463–494. https://doi:10.3934/matersci.2024024
52. Fang J, Zhang L, Sutton D, et al. (2012) Needleless melt-electrospinning of polypropylene nanofibres. *J Nanomater* 2012: 382639. https://doi.org/10.1155/2012/382639
53. Niu P, Liu B, Wei X, et al. (2011) Study on mechanical properties and thermal stability of polypropylene/hemp fiber composites. *J Reinf Plast Compos* 30: 36–44. https://doi.org/10.1177/0731684410383067
54. Xie XL, Fung KL, Li RKY, et al. (2002) Structural and mechanical behavior of polypropylene/maleated styrene-(ethylene-co-butylene)-styrene/sisal fiber composites prepared by injection molding. *J Polym Sci Part B Polym Phys* 40: 1214–1222. https://doi.org/10.1002/polb.10175
55. Hillam L (2004) Alcohol and temperance in modern history: An international encyclopaedia. *Ref Rev* 18: 18–19. https://doi.org/10.1108/09504120410552480
56. Sun T, Luo W, Luo Y, et al. (2020) Self-reinforced polypropylene/graphene composite with segregated structures to achieve balanced electrical and mechanical properties. *Ind Eng Chem Res* 59: 11206–11218. https://doi.org/10.1021/acs.iecr.0c00825
57. Wang X, Kalali EN, Wan JT, et al. (2017) Carbon-family materials for flame retardant polymeric materials. *Prog Polym Sci* 69: 22–46. https://doi.org/10.1016/j.progpolymsci.2017.02.001
58. Al-Saleh MA, Yussuf AA, Al-Enezi S, et al. (2019) Polypropylene/graphene nanocomposites: Effects of GNP loading and compatibilizers on the mechanical and thermal properties. *Materials (Basel)* 12: 3924. https://doi.org/10.3390/ma12233924
59. El Achaby M, Arrakhiz F, Vaudreuil S, et al. (2012) Mechanical, thermal, and rheological properties of graphene-based polypropylene nanocomposites prepared by melt mixing. *Polym Compos* 33: 733–744. https://doi.org/10.1002/pc.22198
60. Feng J, Safaei B, Qin Z, et al. (2023) Bio-inspired metallic cellular material with extraordinary energy dissipation capability. *Chem Eng J* 475: 146382. https://doi.org/10.1016/j.cej.2023.146382
61. Görbe Á, Varga LJ, Bárány T (2023) Development of nanoparticle-filled polypropylene-based single polymer composite foams. *Heliyon* 9: e19638. https://doi.org/10.1016/j.heliyon.2023.e19638

62. Ahmad SR, Xue C, Young RJ (2017) The mechanisms of reinforcement of polypropylene by graphene nanoplatelets. *Mater Sci Eng B* 216: 2–9. https://doi.org/10.1016/j.mseb.2016.10.003